SACLANTCEN REPORT
serial no.: SR-145

SACLANT UNDERSEA
RESEARCH CENTRE

REPORT

A model for the generation of noise by bubbles formed in breaking waves

R.M. Heitmeyer
and R.D. Hollett

August 1988

The SACLANT Undersea Research Centre provides the Supreme Allied Commander Atlantic (SACLANT) with scientific and technical assistance under the terms of its NATO charter, which entered into force on 1 February 1963. Without prejudice to this main task—and under the policy direction of SACLANT—the Centre also renders scientific and technical assistance to the individual NATO nations.

Page count for SR-145
(excluding covers)

Pages	Total
i–vi	6
1–38	38
	44

SACLANT Undersea Research Centre
Viale San Bartolomeo 400
19026 San Bartolomeo (SP), Italy

tel: 0187 540 111
telex: 271148 SACENT I

NORTH ATLANTIC TREATY ORGANIZATION

A model for the generation of noise by bubbles formed in breaking waves

R.M. Heitmeyer and R.D. Hollett

The content of this document pertains to work performed under Project 21 of the SACLANTCEN Programme of Work. The document has been approved for release by The Director, SACLANTCEN.

Peter C. Wille
Director

intentionally blank page

A model for the generation of noise by bubbles formed in breaking waves

R.M. Heitmeyer and R.D. Hollett

Executive Summary: The characteristics of the ambient noise field in the sea are important to the performance prediction, detection capabilities and optimum use of sonar systems. Recognising this, the aim of ambient noise studies at SACLANTCEN is to improve knowledge and prediction of the ambient noise field in areas of importance. These studies involve the development and validation of models for the generation and distribution of the noise.

This report presents a model for the generation of high-frequency, wind-related noise. The model is based on the assumption that the noise is generated by air bubbles entrained in whitecaps (breaking waves). The characteristics of the noise predicted by the model compare favourably with published observations, regarding directionality, level and spectral form.

The development of the model involves a statistical approach in terms of the individual bubbles rather than a continuum approach in terms of an air/water mixture.

This work concludes the theoretical modelling of high-frequency, wind-related noise conducted at the Centre. The results contribute to progress in identifying the sources of wind-related noise in the sea. A later report will present the results of experimental observations of the noise from whitecaps at sea.

intentionally blank page

A model for the generation of noise by bubbles formed in breaking waves

R.M. Heitmeyer and R.D. Hollett

Abstract: A general model is presented that describes the high-frequency noise cross-spectrum generated by the vibrations of bubbles formed in breaking waves. The bubble vibrations are described as linear with the excitation occurring at the moment the bubble is formed. Two simplified models are obtained from the general model under idealized propagation assumptions. The simplified models can be viewed as extensions of the Kuperman and Ingenito and the Cron and Sherman models in that the source mechanism is included. To obtain specific results we postulate that the bubble vibrations are excited either by a rapid pressure change at formation or by an initial rate of change of the bubble volume. The noise intensity spectra for these two excitation mechanisms are evaluated over the frequency range 0.66–10 kHz using one of the simplified models with the parameters estimated for a particular wind speed. Although different, both spectra have levels comparable to the Wenz spectrum for the same wind speed.

Keywords: breaking waves o bubble vibrations o wind-related noise

Contents

1. Introduction

In his classical paper, Wenz [1] speculated that two likely sources of high-frequency, wind-related noise are spray and bubbles. Spray is generated by the action of the wind on the crests of waves and by wave breaking. Bubbles are generated in large numbers by the entrainment of air in breaking waves. Air entrainment following the impact of spray also generates bubbles. A number of authors have developed models for the high-frequency noise generated by spray impact or bubble vibrations. The spray impact model of Wilson [2] is an empirical model based on Franz's measurements [3] of the sound generated by the impact of sprays in a water tank. To rigorously quantify the relative contribution of spray impact noise, further work must be done on the amount of spray generated and the characteristics of that spray (droplet size, impact speed and angle). Kerman [4] has developed a model for the noise generated by non-linear vibrations of the bubbles in breaking waves. The assumption is made that the turbulence in breaking waves is sufficiently strong to force non-linear vibrations of the entrained bubbles. Other models that are also based on non-linear motion of the bubble wall are those of Furduev [5] and Shang and Anderson [6]. Whether or not non-linear motion of the bubble wall really occurs remains to be determined. Crowther [7] has developed a semi-empirical model in which the noise is generated by linear vibrations of the bubbles excited at formation. In his model the source level is determined empirically from the noise spectra of bubbles formed following spray impact in a tank.

In this report we present a model for the noise generated by the linear vibrations of the bubbles formed in breaking waves where the vibrations are assumed to be excited at the moment the bubble is formed. General expressions are presented for the cross-spectra of the noise produced by an individual breaking wave and the noise produced by the aggregate of the breaking waves. The spectra for a single hydrophone are obtained as special cases of the cross-spectra. We then present two simplified models for the cross-spectra obtained under idealized propagation assumptions. Both the general and the simplified models are applicable to an arbitrary bubble excitation mechanism. To obtain specific results we postulate that the bubble vibrations are excited either by a rapid change in the pressure on the bubble wall at the moment of formation or by an initial rate of change of the bubble volume. The noise intensity spectra for these two excitation mechanisms are evaluated over the frequency range 0.66–10 kHz using one of the simplified models and the results are compared to a Wenz spectrum.

2. The general model

The sound produced by the linear vibrations of a bubble is well understood. The pressure waveform is determined from the second time derivative of the volume vibrations which in turn are determined as the solution of a second-order linear differential equation with constant coefficients [8,9]. Accordingly, the spectrum of the pressure observed at some reference distance x_0 can be written as the product

$$P_b(\omega) = H(\omega)F(\omega), \tag{1}$$

where $H(\omega)$ is the pressure transfer spectrum and $F(\omega)$ is the pressure excitation spectrum. The pressure transfer spectrum is equal to the bubble pressure spectrum when the bubble is excited by an impulse excitation of unit strength. This spectrum is given by

$$H(\omega) = \frac{-(R/x_0)\omega^2}{-(\omega^2 - \omega_0^2) + i\delta\omega_0\omega}, \tag{2}$$

where R is the equilibrium radius of the bubble, $\omega_0 = 2\pi f_0$, is the natural angular frequency of the monopole bubble vibrations, and δ is the damping constant. For bubble radii of interest here, ω_0 and δ are well approximated [9,10] by

$$\omega_0 = 2\pi(3.3 \text{ m s}^{-1})/R, \tag{3a}$$

$$\delta = 0.014 + 1.8 \times 10^{-4}\omega_0^{1/2}. \tag{3b}$$

The pressure transfer spectrum for the radii of interest is dominated by a large peak that occurs for $\omega \approx \omega_0$, with a value approximately given by $R/\delta x_0$. The pressure excitation spectrum describes both the applied pressure on the bubble wall and the departure from the equilibrium state at the time at which the bubble is caused to vibrate. This spectrum is given by

$$F(\omega) = (\rho/4\pi R)\left(i\omega\Delta V(0) + \dot{V}(0)\right) - \Delta P(\omega), \tag{4}$$

where $\Delta V(0) = V(0) - V_0$, is the initial volume displacement, $V_0 = \frac{4}{3}\pi R^3$, is the equilibrium volume of the bubble, $\dot{V}(0)$ is the initial volume rate, and $\Delta P(\omega)$ is the spectrum of the pressure excess acting on the bubble wall. The initial volume displacement is equivalent to an excitation by a doublet (the time derivative of an impulse), and the initial volume rate is equivalent to an impulse excitation. Thus, the first term has a significant spectral component at the natural bubble frequency and hence gives rise to high-frequency sound. This term is non-zero whenever a bubble is formed in a non-equilibrium state. The pressure-excess term has significant energy at the natural bubble frequency if, at the moment of formation, the excess pressure waveform changes significantly over a time period of the order of $2\pi/\omega_0$. Whether

the bubble is excited by formation in a non-equilibrium state or by a rapid change in excess pressure at formation, the resulting excess energy is, in part, emitted in the form of a damped pressure wave. The spectrum of the pressure wave observed at any point is determined as the product of the spectrum $4\pi x_0 P_b(\omega)$ and the appropriate Green function. In what follows we omit the reference distance x_0 with the understanding that unit distance is implied.

A physical picture for the formation of the bubbles that produce the sound is provided by the description of a spilling breaker by Longuet-Higgins and Turner [11]. According to these authors, the whitecap formed on a spilling breaker can be regarded as a turbulent air/water mixture that is both accelerated down the forward slope of the wave by gravity and retarded by the entrainment of upslope momentum from the flow in the wave below. This air/water mixture is lighter than the water in the wave below owing to the entrainment of air bubbles and remains distinct from the rest of the wave. Bubbles are generated at the front of the whitecap by the over-running of a layer of air as the front advances and they are generated along the surface of the whitecap by the trapping of air under the turbulent eddies which break out of the surface of the whitecap. We consider only those bubbles that are generated at the whitecap front - not those that are generated along the surface of the whitecap itself.

The model for the cross spectrum of the noise generated by a breaking wave is based on two fundamental assumptions. Firstly, neither the sound produced by an individual bubble nor the propagation of that sound to the hydrophones is influenced by the presence of the other bubbles in the breaking wave. Stated in other terms, the bubbles in the breaking wave do not vibrate collectively to produce the sound and the propagation of the sound from an individual bubble is not absorbed or scattered by the other bubbles in the breaking wave. Secondly, the number of bubbles generated in the breaking wave and the positions and times at which those bubbles are generated are described by a Poisson process. Furthermore the equilibrium radii of those bubbles are statistically independent with a probability density that depends only on the bubble occurrence position.

The setting for the model is illustrated in Fig. 1. The breaking wave occurs at position $\mathbf{r}$ and time τ and the sound produced by that wave is observed on hydrophones located at positions $\mathbf{z}_1$ and $\mathbf{z}_2$. The bubbles are generated in a region located at the front of the whitecap that advances with the whitecap front down the leading face of the breaking wave. The total volume swept out by the bubble generation region during the lifetime of the breaking wave is the source region V. The total number of bubbles generated in the source region is N_b and the positions and times at which those bubbles are generated are $\{(\mathbf{y}_k, \nu_k), k = 1, \ldots, N_b\}$, where ν_k is measured relative to the breaking-wave occurrence time τ. The damped pressure wave emitted by each bubble is of sufficiently short duration that the effect of buoyancy and transport of the bubble in the turbulence is neglected. By the first assumption the spectrum of the pressure observed on each hydrophone from all of the bubbles

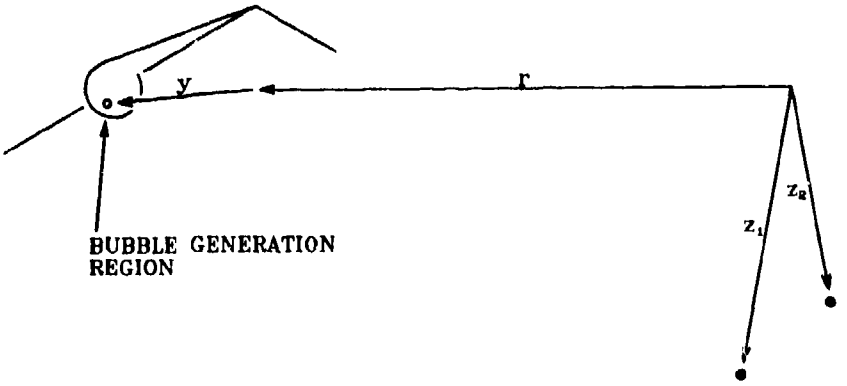

Fig. 1. The physical setting for the general model.

generated in the breaking wave is the superposition of the received pressure spectra from each of the bubbles. Thus using the linear theory to describe the received pressure spectrum from each bubble, the spectrum of the total pressure observed on each hydrophone can be written in the form

$$P_w(\omega; \mathbf{r}, \mathbf{z}_j) = \sum_{k=1}^{N_b} P_b(\omega; \mathbf{y}_k, R_k) G(\omega, \mathbf{r} + \mathbf{y}_k, \mathbf{z}_j) e^{i\omega\nu_k}, \tag{5}$$

where $P_b(\omega; \mathbf{y}, \Re)$ is the pressure spectrum for a bubble generated at position $\mathbf{y}$ with equilibrium radius R and $G(\omega, \mathbf{r} + \mathbf{y}, \mathbf{z}_j)/4\pi$ is the Green function describing the propagation from the bubble position $\mathbf{r} + \mathbf{y}$ to the hydrophone positions $\mathbf{z}_1$ and $\mathbf{z}_2$. For fixed values of $\mathbf{y}$, ν and R, the Green function and the pressure transfer spectrum $H(\omega; \mathbf{y}, R)$ are assumed to be deterministic; the pressure excitation spectrum $F(\omega; \mathbf{y}, R)$ is, in general, stochastic with cross-spectrum

$$C_F(\omega; \mathbf{y}, \mathbf{y}', R, R') = E_b[F^*(\omega; \mathbf{y}, R) F(\omega; \mathbf{y}', R')] \tag{6a}$$

and energy spectrum

$$S_F(\omega; \mathbf{y}, R) = E_b[|F(\omega; \mathbf{y}, R)|^2], \tag{6b}$$

where $E_b[\cdot]$ is the expected value operator for fixed values of the bubble occurrences and the bubble radii.

The Poisson process describes the generation of bubbles by the ensemble of breaking waves that occur at the position $\mathbf{r}$. This process is specified by a bubble generation rate $\mu(\mathbf{y}, \nu)$ that represents the mean number of bubbles that are generated per unit volume per unit time in the bubble generation region during the breaking-wave

lifetime. The mean number generated per unit volume at the point $\mathbf{y}$ in the source region V is given by the bubble generation rate

$$\mu(\mathbf{y}) = \int_0^\infty \mu(\mathbf{y}, \nu)\, \mathrm{d}\nu, \tag{7a}$$

and the mean number of bubbles is

$$M_\mathrm{b} = \int_V \mu(\mathbf{y})\, \mathrm{d}^3\mathbf{y}, \tag{7b}$$

where $\mathrm{d}^3\mathbf{y}$ is the volume element. Finally the equilibrium radii of the bubbles generated at the position $\mathbf{y}$ are described by the bubble-radius probability density $p(R \mid \mathbf{y})$. For reference purposes, the properties of Poisson processes relevant to this report are summarized in Appendix A.

The breaking-wave cross-spectrum is the mean cross-spectrum of the pressure observed at $\mathbf{z}_1$ and $\mathbf{z}_2$ for all breaking waves that occur at the position $\mathbf{r}$. In Appendix C it is shown that this cross-spectrum can be written as the sum of two cross-spectra. The first is the cross-spectrum that results if the received pressure contributions from the individual bubbles were statistically uncorrelated with zero mean. The second cross-spectrum includes the effects of both the non-zero mean and the correlation in the received pressure contributions that results from the correlation in the bubble excitation spectra (see (6a)). In Appendix D we derive an upper bound on the energy contribution of the second spectrum relative to that of the first. By evaluating this upper bound we show that the first spectrum makes the dominant contribution at the high frequencies of interest in this report. On the basis of this result we henceforth neglect the contribution of the second cross-spectrum. With this approximation, the breaking-wave cross-spectrum can be written in the form

$$C_\mathrm{w}(\omega; \mathbf{r}, \mathbf{z}_1, \mathbf{z}_2) = M_\mathrm{b} S_\mathrm{m.b.}(\omega) C_\mathrm{p}(\omega; \mathbf{r}, \mathbf{z}_1, \mathbf{z}_2), \tag{8a}$$

where $S_\mathrm{m.b.}(\omega)$ is the mean bubble spectrum and $C_\mathrm{p}(\omega; \mathbf{r}, \mathbf{z}_1, \mathbf{z}_2)$ is the propagation cross-spectrum. The mean bubble spectrum is given by

$$S_\mathrm{m.b.}(\omega) = M_\mathrm{b}^{-1} \int_V \mu(\mathbf{y}) S_\mathrm{r.b.}(\omega; \mathbf{y})\, \mathrm{d}^3\mathbf{y}, \tag{8b}$$

where

$$S_\mathrm{r.b.}(\omega; \mathbf{y}) = \int_0^\infty S_\mathrm{b}(\omega; \mathbf{y}, R) p(R \mid \mathbf{y})\, \mathrm{d}R \tag{8c}$$

is the radius-averaged bubble spectrum and

$$S_\mathrm{b}(\omega; \mathbf{y}, R) = |H(\omega; \mathbf{y}, R)|^2 S_F(\omega; \mathbf{y}, R) \tag{8d}$$

is the single-bubble spectrum. The propagation cross-spectrum is given by

$$C_\mathrm{p}(\omega; \mathbf{r}, \mathbf{z}_1, \mathbf{z}_2) = \int_V \hat{S}_\mathrm{r.b.}(\omega; \mathbf{y}) G^*(\omega, \mathbf{r} + \mathbf{y}, \mathbf{z}_1) G(\omega, \mathbf{r} + \mathbf{y}, \mathbf{z}_2)\, \mathrm{d}^3\mathbf{y}, \tag{8e}$$

where

$$\hat{S}_{\text{r.b.}}(\omega;\mathbf{y}) = \frac{\mu(\mathbf{y})S_{\text{r.b.}}(\omega;\mathbf{y})}{\int_V \mu(\mathbf{y})S_{\text{r.b.}}(\omega;\mathbf{y})\,\mathrm{d}^3\mathbf{y}} \tag{8f}$$

is the normalized radius-averaged spectrum. The complete equation for the breaking-wave cross-spectrum can be found in Appendix C.

The cross-spectrum of (8a) can be interpreted as follows. The propagation cross-spectrum $C_{\text{p}}(\omega;\mathbf{r},\mathbf{z}_1,\mathbf{z}_2)$ is the cross-spectrum of the pressure from a volume distribution of uncorrelated, zero-mean monopole sources where the energy emitted by each source is described by the normalized radius-averaged spectrum $\hat{S}_{\text{r.b.}}(\omega;\mathbf{y})$. By virtue of (8f) the energy spectrum level for the volume distribution is normalized to unity. The single-bubble spectrum $S_{\text{b}}(\omega;\mathbf{y},R)$ describes the energy emitted by a bubble that is generated at position $\mathbf{y}$ with an equilibrium radius R. The radius-averaged spectrum $S_{\text{r.b.}}(\omega;\mathbf{y})$ is the average of the single-bubble spectrum with respect to the radius probability density $p(R \mid \mathbf{y})$; i.e. it describes the average energy emitted by a single bubble located at the position $\mathbf{y}$ as the radius of that bubble ranges through all possible values. The quantity $M_{\text{b}}^{-1}\mu(\mathbf{y})$ is the probability density on the bubble occurrence positions (see Appendix A). The mean bubble spectrum $S_{\text{m.b.}}(\omega)$ is the average of $S_{\text{r.b.}}(\omega;\mathbf{y})$ with respect to this probability density. Thus the mean bubble spectrum describes the average energy emitted by a single bubble located anywhere in the source region V as both the radius and the position of that bubble range through all possible values. Finally since M_{b} is the mean number of bubbles generated in the source region, the spectrum $M_{\text{b}}S_{\text{m.b.}}(\omega)$ describes the average energy emitted by all of the bubbles in a breaking wave. With these interpretations (8a) indicates that the breaking-wave cross-spectrum is determined as the product of a spectrum that describes the average energy of the sound emitted by a breaking wave and a cross-spectrum that describes the propagation of that sound from the position of the breaking wave to the hydrophone positions.

The noise cross-spectrum is defined as the fourier transform of the cross-correlation function of the pressure due to the aggregate of the breaking waves on the ocean surface. The expression for the noise cross-spectrum is obtained under two assumptions: firstly, that the pressure waveforms received at the hydrophones from different breaking waves are statistically independent and identically distributed; and secondly, that the occurrence positions and occurrence times of the breaking waves $\{(\mathbf{r}_k,\tau_k)\}$ are described by a second Poisson process that is independent of the bubble generation process. This process is determined by a breaking-wave occurrence rate $\lambda(\mathbf{r})$ that represents the mean number of breaking-wave occurrences per unit area of the ocean surface per unit time at the position $\mathbf{r}$. From these assumptions it is shown in Appendix B that the noise cross-spectrum is given by

$$C(\omega;\mathbf{z}_1,\mathbf{z}_2) = \int_{A_s} \lambda(\mathbf{r})C_{\text{w}}(\omega;\mathbf{r},\mathbf{z}_1,\mathbf{z}_2)\,\mathrm{d}^2\mathbf{r}, \tag{9}$$

where $d^2\mathbf{r}$ is the surface area element and A_s is the total area of the ocean surface over which the breaking waves occur. This equation indicates that the noise cross-spectrum is obtained as the integral over the ocean surface of the mean cross-spectrum of the pressure from a single breaking wave weighted by the breaking-wave occurrence rate. Note that this result is the same as would be obtained if the field of individual breaking waves were viewed as a continuum on the ocean surface. It is emphasized, however, that (9) is a consequence of the Poisson assumption and does not result from a continuum approximation. Such an approximation would not be plausible in the light of the sparsity with which breaking waves occur on the ocean surface.

For the high frequencies of interest in this report the noise cross-spectrum is well approximated by using (8) to substitute for the breaking-wave cross-spectrum in (9). The resulting noise cross-spectrum can be written in the form

$$C(\omega; \mathbf{z}_1, \mathbf{z}_2) = M_b S_{\text{m.b.}}(\omega) C_{\text{i.p.}}(\omega; \mathbf{z}_1, \mathbf{z}_2), \tag{10a}$$

where

$$C_{\text{i.p.}}(\omega; \mathbf{z}_1, \mathbf{z}_2) = \int_{A_s} \lambda(\mathbf{r}) C_p(\omega; \mathbf{r}, \mathbf{z}_1, \mathbf{z}_2)\, d^2\mathbf{r} \tag{10b}$$

is referred to here as the integrated propagation cross-spectrum. To interpret these equations we note that the noise cross-spectrum can be expressed as the integral over the surface region of the product of the spectrum $\lambda(\mathbf{r}) M_b S_{\text{m.b.}}(\omega)$ and the propagation cross-spectrum $C_p(\omega; \mathbf{r}, \mathbf{z}_1, \mathbf{z}_2)$. As noted previously the spectrum $M_b S_{\text{m.b.}}(\omega)$ is the mean energy spectrum for the breaking waves that occur at the position $\mathbf{r}$, and $\lambda(\mathbf{r})$ is the rate per unit surface area per unit time at which these breaking waves occur. It follows that the product $\lambda(\mathbf{r}) M_b S_{\text{m.b.}}(\omega)$ is the mean intensity source spectrum per unit area for the succession of breaking waves that occur at $\mathbf{r}$. Consequently, the product of this source spectrum with the propagation spectrum $C_p(\omega; \mathbf{r}, \mathbf{z}_1, \mathbf{z}_2)$ is the noise cross-spectrum per unit area for the breaking waves that occur at $\mathbf{r}$. Thus (10a) and (10b) state that the noise cross-spectrum for all breaking waves is obtained as the integral of the noise cross-spectrum for the breaking waves that occur at each point on the surface region.

3. The simplified models

In the noise model the propagation of the sound to the hydrophone positions is described by the two cross-spectra $C_p(\omega; \mathbf{r}, \mathbf{z}_1, \mathbf{z}_2)$ and $C_{i.p.}(\omega; \mathbf{z}_1, \mathbf{z}_2)$. The propagation cross-spectrum $C_p(\omega; \mathbf{r}, \mathbf{z}_1, \mathbf{z}_2)$ describes the sound propagation from all points in the source region of a breaking wave located at the position $\mathbf{r}$; the integrated cross-spectrum $C_{i.p.}(\omega; \mathbf{z}_1, \mathbf{z}_2)$ describes the sound propagation from all breaking-wave positions. A considerable simplification in the noise model results if the acoustic propagation is appoximated as that determined for a source region lying below a flat, pressure-release surface. With this approximation the integrated cross-spectrum can be obtained from an extension of the noise-propagation model of Kuperman and Ingenito [12], provided that the source region has a horizontal cross-section that is independent of the vertical coordinate, and that the medium is horizontally stratified (i.e. the sound speed and bottom characteristics are independent of the horizontal coordinates). If, in addition, the medium can be viewed as homogeneous and semi-infinite (constant sound speed and no bottom) the integrated cross-spectrum can be obtained from an extension of the Cron and Sherman model [13]. In this section we describe the simplified models that result from these approximations.

The setting for the simplified models is illustrated in Fig. 2. We take the surface region A_s to be of infinite extent and assume that the breaking-wave occurrence rate $\lambda(\mathbf{r})$ is independent of $\mathbf{r}$. The source region extends down from the surface to a depth D with a horizontal cross-section A' that is independent of depth. Within the source region, the bubble position vector $\mathbf{y}$ is represented as the sum of a horizontal vector $\mathbf{y}'$ and a vertical vector $\mathbf{y}''$ with magnitude $y'' \in [0, D]$. The two hydrophones are located at positions $\mathbf{z}_1$ and $\mathbf{z}_2$. In the ideal medium case (homogeneous, semi-infinite) the hydrophones are assumed to be located far enough below the ocean surface that the incident acoustic field can be viewed as planewave. For this case, the vertical vector $\mathbf{z}$, of magnitude z, points to the midpoint of the line connecting the hydrophones. The positions of the hydrophones relative to the midpoint are determined by the hydrophone difference vector $\mathbf{z}' = \mathbf{z}_2 - \mathbf{z}_1$, that has magnitude z' and lies at an angle γ relative to the horizontal plane. The planewave field is described by the wavenumber vector $\mathbf{k}$ that has magnitude $k = \omega/c$, and points in the direction of $\mathbf{z} - \mathbf{r}$ at an angle θ relative to the vertical.

In the stratified medium case, the noise cross-spectrum is obtained from the general model using the integrated cross-spectrum that results from the simplifying assumptions. To obtain the integrated cross-spectrum, we use the propagation cross-spectrum of (8e) in (10b), interchange the order of the surface and the volume integrations, and express the volume integral as an integral over the horizontal cross-sectional area followed by an integral over the depth interval. (This last step

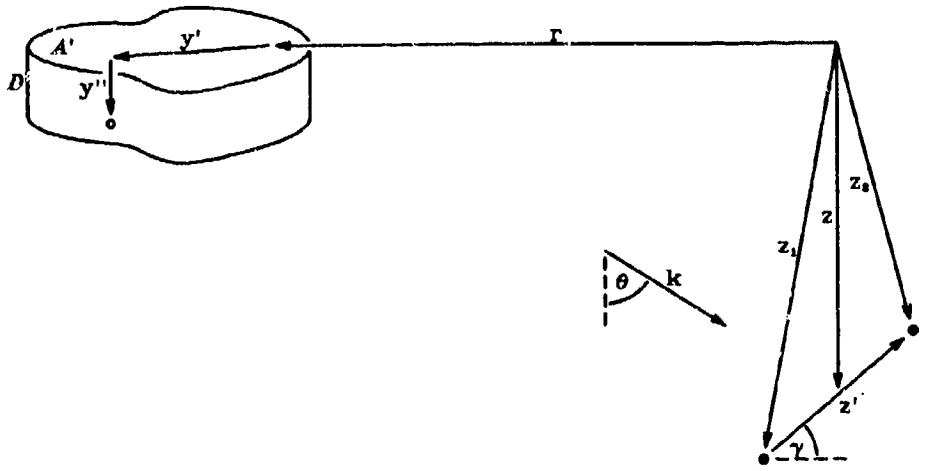

Fig. 2. Setting for the simplified models.

is permitted by the assumption on the form of the source region.) The result is

$$C_{\text{i.p.}}(\omega;\mathbf{z}_1,\mathbf{z}_2) = \lambda \int_0^D \int_{A'} \hat{S}_{\text{r.b.}}(\omega;\mathbf{y}'+\mathbf{y}'') \times \int_{A_s} G^*(\omega,\mathbf{r}+\mathbf{y}'+\mathbf{y}'',\mathbf{z}_1) G(\omega,\mathbf{r}+\mathbf{y}'+\mathbf{y}'',\mathbf{z}_2)\,\mathrm{d}^2\mathbf{r}\,\mathrm{d}^3\mathbf{y}. \quad (11)$$

The final expression for the integrated cross-spectrum is obtained by making the change of variable $\mathbf{r}' = \mathbf{r}+\mathbf{y}'$ in the surface integral of (11) and using the assumption that A_s has infinite extent to eliminate the dependence on the horizontal vector $\mathbf{y}'$. The noise cross-spectrum is then obtained by substituting in (10a). The result can be written in the form

$$C(\omega;\mathbf{z}_1,\mathbf{z}_2) = \lambda M_{\text{b}} S_{\text{m.b.}}(\omega) C'_{\text{i}}(\omega;\mathbf{z}_1,\mathbf{z}_2), \quad (12a)$$

where

$$C'_{\text{i}}(\omega;\mathbf{z}_1,\mathbf{z}_2) = \int_0^D \hat{S}_{\text{r.b.}}(\omega;y'') C'(\omega;y'',\mathbf{z}_1,\mathbf{z}_2)\,\mathrm{d}y'' \quad (12b)$$

and

$$\hat{S}_{\text{r.b.}}(\omega;y'') = \int_{A'} \hat{S}_{\text{r.b.}}(\omega;\mathbf{y}'+\mathbf{y}'')\,\mathrm{d}^2\mathbf{y}', \quad (12c)$$

$$C'(\omega;y'',\mathbf{z}_1,\mathbf{z}_2) = \int_{A_s} G^*(\omega,\mathbf{r}+\mathbf{y}'',\mathbf{z}_1) G(\omega,\mathbf{r}+\mathbf{y}'',\mathbf{z}_2)\,\mathrm{d}^2\mathbf{r}. \quad (12d)$$

Note that $C_i'(\omega; \mathbf{z}_1, \mathbf{z}_2)$ is the integrated cross-spectrum that results for a breaking-wave occurrence rate of unity.

The simplified model of Eqs. (12) determines the noise cross-spectrum as the product of the source spectrum $\lambda M_b S_{m.b.}(\omega)$ and the integrated cross-spectrum $C_i'(\omega; \mathbf{z}_1, \mathbf{z}_2)$. According to (12b), the integrated cross-spectrum is obtained as a depth average of the cross-spectrum $C'(\omega; y'', \mathbf{z}_1, \mathbf{z}_2)$ weighted by the depth-dependent spectrum $\hat{S}_{r.b.}(\omega; y'')$. The cross-spectrum $C'(\omega; y'', \mathbf{z}_1, \mathbf{z}_2)$ is equivalent to that obtained in the Kuperman and Ingenito model for a sheet of spatially-uncorrelated monopole sources located at a depth y'' below the surface. (To see this, make the change of variables $\boldsymbol{\rho} = \mathbf{r}' - \mathbf{r}''$ in Eq. (7) of [12], and take the sources to be uncorrelated by using Eq. (17) of [12], to obtain (12d).) Thus the above simplified model provides both an expression for the source spectrum of the Kuperman and Ingenito model and a rule for combining the 'source-sheet' cross-spectra determined by their model to produce the total noise cross-spectrum. Examples showing the response of an array determined from the 'source-sheet' cross-spectrum of Kuperman and Ingenito for different acoustic environments can be found in Hamson [14].

In the ideal medium case the resulting simplified model provides expressions for both the breaking-wave cross-spectrum and the noise cross-spectrum. These expressions are obtained from the general model with the propagation cross-spectrum and the integrated cross-spectrum determined from the Green function for the ideal medium. Using the method of images the Green function can be obtained by replacing the point source in the semi-infinite medium by a dipole source in an infinite medium where the dipole axis is perpendicular to the surface and the length of the dipole is twice the bubble depth. It follows immediately that the function $G(\omega, \mathbf{r} + \mathbf{y}, \mathbf{z}_j)$ is given by

$$G(\omega, \mathbf{r} + \mathbf{y}, \mathbf{z}_j) = 2i \sin(k'' y'') e^{-i\mathbf{k}\cdot\mathbf{z}_j} \frac{e^{-\alpha|\mathbf{z}-\mathbf{r}|/2}}{|\mathbf{z}-\mathbf{r}|}, \tag{13}$$

where α is a frequency-dependent absorption coefficient and k'' is the vertical component of $\mathbf{k}$. The breaking-wave cross-spectrum is obtained by first using (13) in (8e) to determine the propagation cross-spectrum and then substituting in (8a). The result can be expressed in the form

$$C_w(\omega; \mathbf{r}, \mathbf{z}_1, \mathbf{z}_2) = M_b S_{m.b.}(\omega) R(\omega, \theta) T(\omega, |\mathbf{z}-\mathbf{r}|) e^{-i\mathbf{k}\cdot\mathbf{s}'}, \tag{14a}$$

where

$$R(\omega, \theta) = \int_0^D \hat{S}_{r.b.}(\omega; y'') \left(2 \sin\left(k \cos(\theta) y''\right)\right)^2 \, dy'' \tag{14b}$$

is a frequency-dependent radiation pattern and

$$T(\omega, |\mathbf{z}-\mathbf{r}|) = \frac{e^{-\alpha|\mathbf{z}-\mathbf{r}|}}{|\mathbf{z}-\mathbf{r}|^2} \tag{14c}$$

is the transmission loss from $\mathbf{r}$ to $\mathbf{s}$. This cross-spectrum is the same as that obtained for a point source that has an energy source spectrum $M_b S_{m.b.}(\omega)$ and a radiation pattern $R(\omega, \theta)$ and that radiates sound into an infinite homogeneous medium.

The noise cross-spectrum is obtained with the integrated cross-spectrum determined from the propagation cross-spectrum for the ideal medium. The integral in (10b) is first expressed in polar coordinates to evaluate the azimuth integral and then converted to an integral with respect to θ by making the change of variables $|\mathbf{r}|/z = \tan(\theta)$. The result is then combined with (10a) to obtain

$$C(\omega; \mathbf{z}_1, \mathbf{z}_2) = \lambda M_b S_{m.b.}(\omega) C_i'(\omega; z, z', \gamma), \tag{15a}$$

where the integrated cross-spectrum $C_i'(\omega; z, z', \gamma)$ is given by

$$C_i'(\omega; z, z', \gamma) = 2\pi \int_0^{\pi/2} R(\omega, \theta) e^{-\left(\alpha z \sec(\theta) + ikz' \sin(\gamma)\cos(\theta)\right)} \times J_0\left(kz' \cos(\gamma)\sin(\theta)\right) \tan(\theta)\, d\theta. \tag{15b}$$

This noise cross-spectrum is the same as that obtained by replacing the ocean surface with a sheet of uncorrelated point sources that radiates sound into an infinite homogeneous medium where each source has an intensity source spectrum per unit area $\lambda M_b S_{m.b.}(\omega)$ and a radiation pattern $R(\omega, \theta)$.

The simplified model of Eqs. (15) is related to the Cron and Sherman model through the real part of the normalized integrated cross-spectrum $\rho(\omega; z, z', \gamma) = \mathrm{Re}\left(C_i'(\omega; z, z', \gamma)/C_i'(\omega; z, 0, \gamma)\right)$. Using Eq. (15b) to calculate $\rho(\omega; z, z', \gamma)$ and comparing the result with Eq. (14) of [13], it is seen that for a lossless medium ($\alpha = 0$), the two cross-spectra are identical if the radiation pattern $R(\omega, \theta)$ is replaced by $\cos^{2m}(\theta)$. Thus this simplified model provides not only a source spectrum for the noise-propagation model of Cron and Sherman but also an expression for the radiation pattern in their model.

Further insight can be obtained by comparing the angular dependence of the radiation pattern $R(\omega, \theta)$ at extreme frequencies with the assumed angular dependence in the radiation pattern of Cron and Sherman. To this end it is noted that the radiation pattern $R(\omega, \theta)$ is obtained as the depth integral of the radiation pattern for a vertical dipole weighted by the depth-dependent spectrum $\hat{S}_{r.b.}(\omega; y'')$. For low frequencies the dipole radiation pattern is approximately that of an infinitesimal dipole for all depths in the source region. Thus the result of the depth integration is an infinitesimal dipole which has the form

$$R(\omega, \theta) = \left(2(\omega/c)\cos(\theta) D'(\omega)\right)^2, \tag{16a}$$

where

$$D'(\omega) = \left(\int_0^D \hat{S}_{r.b.}(\omega; y'')(y'')^2\, dy''\right)^{1/2}. \tag{16b}$$

It follows that for low frequencies the cross-spectrum $\rho(\omega; z, z', \gamma)$ is approximately that of the Cron and Sherman model for $m = 1$. For high frequencies the dipole radiation pattern for a bubble at a particular depth has multiple lobes that occur in directions which vary with the depth of the bubble. Thus the dipole radiation pattern for a bubble at one depth has lobes that occur in the directions of the nulls in the radiation pattern for a bubble at another depth. The effect of the depth integration in (14b) is to produce a radiation pattern that is approximately constant over all angles for which the multiple lobes occur. This can be seen in more formal terms by rewriting (14b) in the form

$$R(\omega, \theta) = 2\left(1 - \int_0^D \hat{S}_{\text{r.b.}}(\omega; y'') \cos\left(2(\omega/c)\cos(\theta)y''\right)\, \mathrm{d}y''\right). \tag{17}$$

For high frequencies the second term in (17) will be negligible provided that $\hat{S}_{\text{r.b.}}(\omega; y'')$ varies slowly with depth in comparison to $\cos\left(2(\omega/c)\cos(\theta)y''\right)$. In the case where $\hat{S}_{\text{r.b.}}(\omega; y'')$ is independent of y'', the second term will be negligible for frequencies and angles satisfying $f > (c/2D)/\cos(\theta')$ and $\theta < \theta'$. For these frequencies and angles, $R(\omega, \theta) \approx 2$. Thus, for sufficiently high frequencies, the radiation pattern is approximately that of a frequency-independent monopole (except for angles near $\frac{1}{2}\pi$), and hence the cross-spectrum $\rho(\omega; z, z', \gamma)$ for $\alpha = 0$ is approximately that of the Cron and Sherman model for $m = 0$. For later reference we note that the integrated spectrum $C_{\text{i}}'(\omega; z, 0, \gamma)$ for $\alpha = 0$ has the frequency dependence $(2(\omega/c)D'(\omega))^2$ at low frequencies and is essentially independent of frequency at high frequencies.

It is important to emphasize that the simplified models are obtained with the source region located below a flat surface. The bubbles that produce the sound, however, are assumed to be located well within the breaking wave itself, and over the frequency band considered, the wavelength of the radiated sound from each bubble is comparable to or smaller than the dimensions of the breaking wave. Consequently the cross-spectra obtained from the simplified models might differ significantly from those obtained if the shape of the breaking wave were taken into account.

4. The excitation postulates

In Sect. 2 it was noted that for linear bubble vibrations excited at formation, high-frequency sound is emitted only if the bubbles are formed in a non-equilibrium state or if the bubbles are subjected to a rapid change in pressure. As stated in Sect. 2, we consider only those bubbles formed as the whitecap front advances, over-running a layer of air. In this section, we postulate two different mechanisms by which the bubble vibrations are excited.

The *first postulate* is essentially a pressure excitation of the bubbles. We assume that at formation, the bubbles are subjected to a rapid pressure increase arising from the weight of the water that over-runs the bubbles. The over-running is assumed to be sufficiently rapid that the pressure increase approximates to a step increase. The pressure excitation spectrum is then given by

$$F(\omega; \mathbf{y}, R) = -i\rho g d(\mathbf{y})/\omega, \tag{18a}$$

and the excitation energy spectrum is

$$S_F(\omega; \mathbf{y}, R) = (\rho g d(\mathbf{y})/\omega)^2, \tag{18b}$$

where $d(\mathbf{y})$ is the depth of the bubble formed at the position $\mathbf{y}$.

The *second postulate* is essentially a volume-rate excitation. At the moment a bubble is formed by the closure of an air cavity we assume that the inward velocity of the water surrounding the cavity imparts an initial volume rate $\dot{V}(0)$ to the bubble. To determine the initial volume rate we use the fact that for the small bubble vibrations for which the linear theory is valid $\dot{V}(0) \approx 4\pi R^2 \dot{R}(0)$, where $\dot{R}(0)$ is the initial radial velocity. By continuity, $\dot{R}(0)$ is equal to the inward velocity of the water at the moment of closure, U. Thus by identifying $\dot{R}(0)$ with U we obtain

$$F(\omega; \mathbf{y}, R) = -\rho R U. \tag{19a}$$

To obtain the excitation energy spectrum we assume that the inward velocity at closure, U, is a random variable with a mean that is independent of the bubble radius and that for any two bubbles, the inward velocities at closure are mutually uncorrelated. These assumptions are equivalent to assuming that at the moment of closure of a cavity, the velocity of the surrounding water is independent of the size of the cavity and that the bubbles are formed with differences in position and time that are large compared with the correlation distance and the correlation time of the turbulent motion in the front. With these assumptions the excitation energy spectrum is given by

$$S_F(\omega; \mathbf{y}, R) = (\rho R U')^2, \tag{19b}$$

where U' is the rms inward velocity at closure.

5. Parameter estimation and model results

In this section we present examples of the mean bubble spectrum $S_{\text{m.b.}}(\omega)$ and the noise intensity spectrum $S(\omega;\mathbf{z}) = C(\omega;\mathbf{z},\mathbf{z})$, for the two excitation postulates described in the previous section. The examples were obtained using the simplified model for the ideal medium with the additional assumption that the bubble generation rate $\mu(\mathbf{y})$, the pressure transfer spectrum of a bubble $H(\omega;\mathbf{y},R)$, and the bubble-radius density $p(R \mid \mathbf{y})$ are independent of the bubble position $\mathbf{y}$ throughout the source region. The simplified model equations for the two excitation postulates are derived with this additional assumption in Appendix E.

The model parameters used for the examples were estimated for a wind speed of 10 m s^{-1}. The estimate of the product λM_b and the form of the bubble-radius density $p(R)$ were based on a model for the generation and distribution of bubbles at the ocean surface proposed by Crowther [15]. In this model the bubbles generated at the ocean surface are distributed by the action of turbulent motions that carry them downwards and by buoyancy that forces them to rise. Under steady-state conditions the number of bubbles per unit volume of radius R that are distributed immediately below the surface is given by

$$n(R) = s(R)/v(R), \tag{20}$$

where $s(R)$ is the number of bubbles per unit area per unit time of radius R that are generated at the surface and $v(R)$ is the rise velocity. From a dimensional argument, Crowther concludes that the surface generation rate $s(R)$ is proportional to $(W/R)^3$, where W is the wind speed. Using this relationship in (20) with an expression for $v(R)$, and fitting the resulting bubble-radius distribution $n(R)$ to backscatter data, he concludes that

$$s(R) \approx 2.3 \times 10^{-10} W^3 R^{-3}. \tag{21}$$

Using this model an expression for λM_b was obtained as follows. Since λ specifies the mean number of breaking waves that occur per unit area of the surface per unit time and M_b specifies the mean number of bubbles generated in a breaking wave, λM_b specifies the mean number of bubbles generated per unit area of the surface per unit time. Assuming that the only significant source of surface-generated bubbles is breaking waves, λM_b is given by the integral of $s(R)$ with respect to R, i.e.

$$\lambda M_b \approx 2.3 \times 10^{-10} W^3 \int_{R_{\min}}^{R_{\max}} R^{-3}\, \mathrm{d}R, \tag{22}$$

where $R_{\min}$ and $R_{\max}$ are the minimum and maximum radii of the bubbles generated in the breaking waves. According to (22) the mean number of bubbles generated in a breaking wave is proportional to the integral of R^{-3} with respect to R and hence

the fraction of these bubbles with radii in $\mathrm{d}R$ is proportional to R^{-3}. It follows that the bubble-radius density is also proportional to R^{-3}, i.e.

$$p(R) \approx R^{-3} / \int_{R_{\min}}^{R_{\max}} R^{-3}\,\mathrm{d}R. \tag{23}$$

The values of $R_{\min}$ and $R_{\max}$ determine the band of natural bubble frequencies in the mean bubble spectrum. The value of $R_{\max}$ was inferred from laboratory measurements of the distribution of bubble radii in simulated breaking waves by Monahan and Zietlow [16]. Over the range of radii from 0.6 mm to 5 mm, their distribution shows an R^{-3} dependence – the same as Crowther's distribution $n(R)$ for a rise velocity that is independent of bubble radius (see (20) and (21)). Some bubbles with radii between 5 and 9 mm were also observed in the laboratory measurements. However, the possibility cannot be excluded that such large bubbles resulted from the coalescence of smaller bubbles formed at some earlier stage. In view of this possibility we restricted $R_{\max}$ to 5 mm, corresponding to a natural bubble frequency of 0.66 kHz. For $R_{\min}$ we used a value of 0.3 mm corresponding to 10 kHz. (We note that the values of $R_{\min}$ and $R_{\max}$ also affect the mean bubble spectrum level owing to the normalization in (23). The noise intensity spectrum level, however, is not affected by these values since the integral in (22) and its inverse in (23) cancel out.)

An estimate of λ was obtained from $\lambda \approx w/A_{\mathrm{m}}T_{\mathrm{m}}$, where w is the fraction of whitecap coverage, and A_{m} and T_{m} are the mean area and mean lifetime of an individual whitecap event. The fraction of whitecap coverage was taken from the observations of Ross and Cardone [17]. In their definition of whitecap coverage, these authors include 'large new foam patches'. This was taken into account in estimating the mean area and lifetime of an individual event. Using the observation $w = 0.01$ for a wind speed of 10 m s^{-1}, with estimates $A_{\mathrm{m}} = 10$ m^2 and $T_{\mathrm{m}} = 10$ s, we obtained $\lambda = 10^{-4}$ breaking waves per square metre of ocean surface per second.

Using the above values of $R_{\min}$, $R_{\max}$ and λ in (22) yielded $M_{\mathrm{b}} = 1.27 \times 10^4$ bubble generations. (We note that for a rectangular bubble generation region 0.2 m (deep)$\times$ 0.2 m$\times$2 m, moving at constant rate during a breaking-wave lifetime of 3 s, 1.27×10^4 bubble generations implies a bubble generation rate $\mu = 5.3 \times 10^4$ bubbles per cubic metre per second. Thus in a cubic decimetre of this moving region 53 bubbles are generated during each second of the breaking-wave lifetime.)

Finally for both excitation postulates, we used a source region depth $D = 0.2$ m, and for the volume-rate postulate, we used an rms inward velocity $U' = 7$ cm s^{-1}.

The mean bubble spectra for the two excitation postulates are illustrated in Fig. 3. Both spectra have their highest energy levels in the frequency band 0.66–10 kHz. This is the band of natural bubble frequencies corresponding to the range of

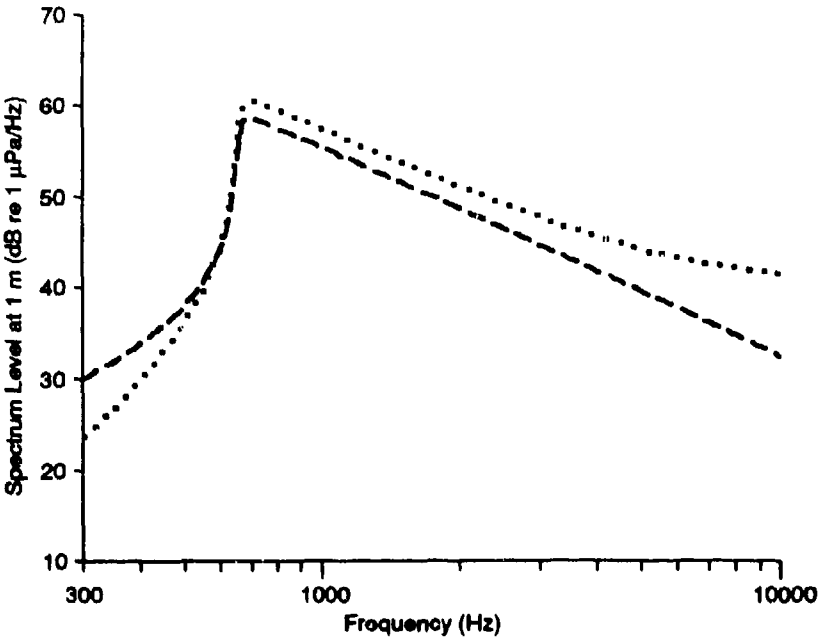

Fig. 3. Mean bubble spectra for 0.2 m source region depth: *dashed curve* – pressure-jump excitation; *dotted curve* – volume-rate excitation for an rms inward velocity of 7 cm s^{-1}.

bubble radii used. Within this band the spectra have comparable levels at the lower frequencies (large bubbles) and both decrease in level as the frequency increases (the bubble radius decreases). The spectra differ from one another in their high-frequency slopes. For the pressure-jump excitation the slope is about −6 dB/octave over the full band, whereas for the volume-rate excitation the slope varies from about −6 dB/octave at the lower frequencies to about −2 dB/octave at the higher frequencies.

To explain the slopes of the mean bubble spectra we first compare the corresponding single-bubble spectra $S_b(\omega; \mathbf{y}, R)$. The shapes of the single-bubble spectra can be seen through the plots of Fig. 4. These plots show the energy transfer spectrum $|H(\omega; R)|^2$ and the excitation energy spectra $S_F(\omega; \mathbf{y}, R)$ for a 3.3 mm radius bubble ($f_0 = 1$ kHz), at the rms source depth; the parameter values are the same as those for the mean bubble spectra of Fig. 3. The shapes of the single-bubble spectra are seen by adding the corresponding excitation spectrum to the transfer spectrum. For both excitation postulates this results in a single-bubble spectrum with a sharp peak at the natural bubble frequency f_0. For the pressure-jump excitation the single-

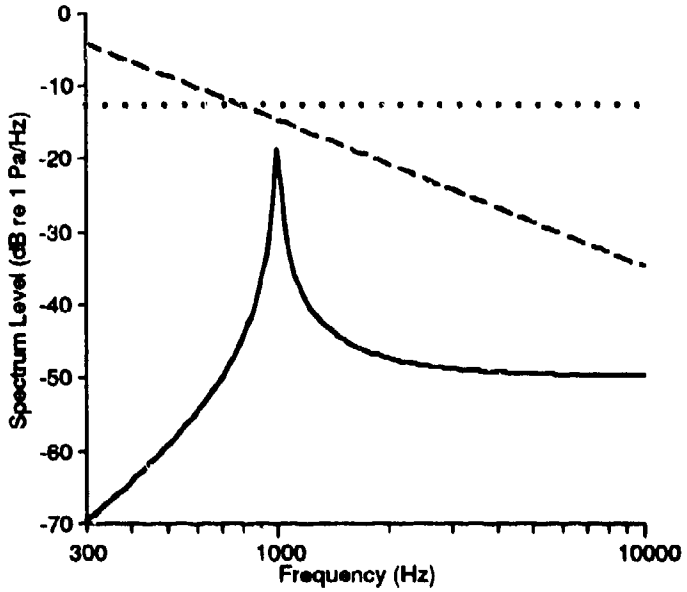

Fig. 4. Single-bubble spectrum components for $R = 3.3$ mm: *solid curve* – energy transfer spectrum at 1 m; *dashed line* – excitation energy spectrum for pressure-jump excitation; *dotted line* – excitation energy spectrum for volume-rate excitation.

bubble spectrum approaches zero for frequencies on either side of f_0 due to the -6 dB/octave slope in the excitation spectrum. In contrast the single-bubble spectrum for the volume-rate excitation only approaches zero for frequencies less than f_0 since the excitation spectrum is flat – for frequencies greater than f_0 the single-bubble spectrum approaches a level that is proportional to R^4. (We note that the peak source level of the single-bubble spectrum for both excitation postulates is roughly 90 dB re 1 μPa at 1 m. This level results from an amplitude of vibration of less than 1% of the equilibrium radius which is well within the linear range.)

Having noted the difference in the shapes of the single-bubble spectra we point out that for both excitation postulates the peak value of the single-bubble spectrum is proportional to $R^4\delta^{-2}$. This can be seen as follows, recalling that the transfer spectrum $|H(\omega;R)|^2$ has a peak of $(R/\delta)^2$. For the volume-rate excitation, $S_F(\omega;\mathbf{y},R) \propto R^2$ so that the peak value of the single-bubble spectrum is proportional to $R^4\delta^{-2}$. For the pressure-jump excitation, $S_F(\omega;\mathbf{y},R) \propto \omega^{-2}$ so that the peak value, which is well approximated by $|H(\omega_0;R)|^2 S_F(\omega_0;\mathbf{y},R)$, is proportional to $(R/\delta)^2\omega_0^{-2}$ or to $R^4\delta^{-2}$. For natural bubble frequencies less than 10 kHz ($R > 0.3$

mm) δ is only weakly dependent on R (see Eqs. (3)), and thus the peak value for both excitations is approximately proportional to R^4.

Having compared the single-bubble spectra the slopes of the mean bubble spectra are explained as follows. For the pressure-jump excitation the single-bubble spectrum goes to zero for frequencies on either side of the sharp peak at ω_0 so that for a fixed frequency ω the major contribution to the integral of (8c) occurs when ω_0 is approximately equal to ω. This occurs for bubble radii $R \approx 2\pi(3.3 \text{ m s}^{-1})/\omega$. For these radii the integrand is approximately equal to the peak value of the single-bubble spectrum weighted by the bubble-radius density. The peak value is proportional to R^4 and the radius density is proportional to R^{-3}. Consequently the integrand is proportional to R so that the integral is proportional to R^2 or equivalently to ω^{-2}, in accordance with the -6 dB/octave slope seen in the mean bubble spectrum of Fig. 3.

For the volume-rate excitation the preceding argument does not apply, even though the peak of the single-bubble spectrum has the same radius dependence as that for the pressure-jump excitation. This is because the single-bubble spectrum does not go to zero for frequencies greater than ω_0, rather it approaches a level that is proportional to R^4. As a result, when ω is large contributions to the integral of (8c) from the single-bubble spectra for small ω_0 (large R) are not small in comparison to those for $\omega_0 \approx \omega$ and hence cannot be neglected. In fact, it is the integration of these contributions that results in the changing slope at high frequencies in the mean bubble spectrum of Fig. 3.

The examples of the noise intensity spectra for the two excitation postulates are shown in Fig. 5. Also shown is the Wenz spectrum for the 10 m s^{-1} wind speed taken from [1]. Both model spectra show a near-constant level at the lower frequencies of the band 0.66–10 kHz, followed by a decrease in level at the higher frequencies. At the lower frequencies the near-constant level in both spectra results from the cancellation of the ω^{-2} dependence in the mean bubble spectrum by the ω^2 dependence in the integrated propagation spectrum (see Sect. 3). At the higher frequencies the slopes of the two model spectra are approximately those of the corresponding mean bubble spectra. This results from the fact that at high frequencies the integrated propagation spectrum is essentially independent of frequency. (For frequencies greater than about 7 kHz, the integrated propagation spectrum decreases with frequency because of the absorption loss – computed for a hydrophone depth of 1000 m – and hence the model noise intensity spectra fall off more rapidly than the corresponding mean bubble spectra.)

The noise intensity spectrum for the pressure-jump excitation shows better agreement with the Wenz spectrum than that for the volume-rate excitation at the high frequencies. At these frequencies the slope of the pressure-jump spectrum is only slightly more negative than the -5 dB/octave slope of the Wenz spectrum, whereas

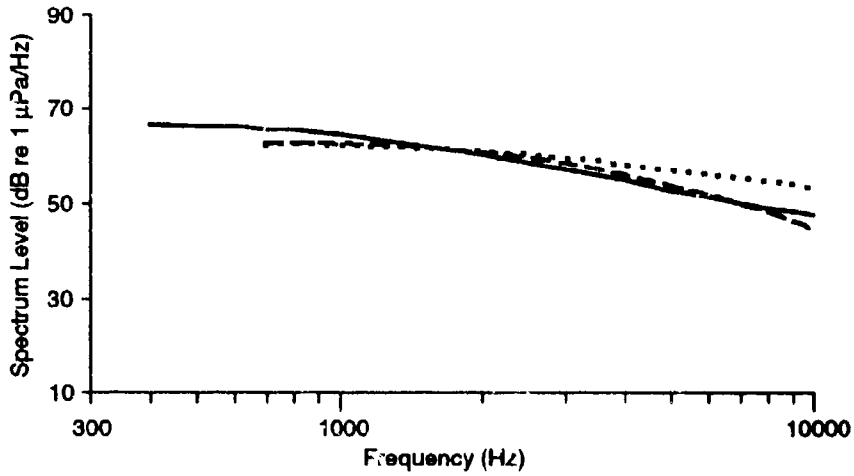

Fig. 5. Noise intensity spectra for 10 m s^{-1} wind speed: *solid curve* - Wenz spectrum; *dashed curve* - pressure-jump excitation and *dotted curve* - volume-rate excitation for $\lambda = 10^{-4}$ breaking waves m^{-2} s^{-1}, $p(R) \propto R^{-3}$, R between 0.3 and 5 mm, $M_b = 1.27 \times 10^4$ bubbles.

the slope of the volume-rate spectrum is at least 2 dB more positive than that of the Wenz spectrum.

6. Summary and conclusion

A general model has been developed for the generation of high-frequency noise by linear vibrations of the bubbles formed in breaking waves. This model essentially comprises two cross-spectra: the breaking-wave cross-spectrum that describes the noise produced by individual breaking waves, and the noise cross-spectrum that describes the noise produced by the aggregate of the breaking waves. The breaking-wave cross-spectrum is obtained by assuming that the noise from the aggregate of bubbles is the superposition of the noise from individual bubbles and that the bubbles are generated according to a Poisson process. This cross-spectrum can be written as the sum of two cross-spectra, one of which makes the dominant energy contribution at high frequencies. The noise cross-spectrum is obtained by assuming that the pressure waveforms from different breaking waves are statistically independent and identically distributed, and that the breaking waves are generated according to a second Poisson process.

Two simplified models have been obtained from the general model by assuming that the source region lies below a flat surface and that the propagation is determined as that for either a stratified medium or an ideal medium. As such, these models can be viewed as extensions of the Kuperman and Ingenito model and the Cron and Sherman model for the case of noise generated by bubbles in breaking waves. Both simplified models characterize the noise source in terms of a spectrum at each point on the ocean surface. For the stratified medium the noise cross-spectrum is obtained from a depth integral of the 'source-sheet' cross-spectrum of the Kuperman and Ingenito model. For the ideal medium the noise cross-spectrum is obtained using a frequency-dependent radiation pattern in the Cron and Sherman model.

Examples of the noise intensity spectra for a 10 m s^{-1} wind speed have been presented for two postulated excitation mechanisms – a pressure-jump excitation and a volume-rate excitation. These spectra were computed using the simplified model for the ideal medium with values of the parameters mostly inferred from published measurements. Although different the two spectra both show levels comparable to the Wenz spectrum for the same wind speed. Of the two spectra, the high-frequency slope of the pressure-jump spectrum is in better agreement with the Wenz spectrum. It is noted, however, that the idealized propagation assumption used in the simplified model neglects the shape of the breaking wave. If this shape were accounted for there would be a different frequency dependence in the radiation pattern which could significantly change the shape of the model spectra at the higher frequencies. It is also noted that there are uncertainties in the overall levels of the model spectra due to uncertainties in the parameters. Nevertheless, the rough agreement between the model spectra and the Wenz spectrum supports the hypothesis that linear vibrations of bubbles generated in breaking waves are a primary source of wind-related noise.

References

[1] WENZ, G.M. Acoustic ambient noise in the ocean: spectra and sources. *Journal of the Acoustical Society of America*, **34**, 1962: 1936–1956.

[2] WILSON, J.H. Low-frequency wind-generated noise produced by the impact of spray with the ocean's surface. *Journal of the Acoustical Society of America*, **68**, 1980: 952–956.

[3] FRANZ, G.J. Splashes as sources of sound in liquids. *Journal of the Acoustical Society of America*, **31**, 1959: 1080–1096.

[4] KERMAN, B.R. Underwater sound generation by breaking wind waves. *Journal of the Acoustical Society of America*, **75**, 1984: 149–165.

[5] FURDUEV, A.V. Undersurface cavitation as a source of noise in the ocean. *Izvestiya Atmospheric and Oceanic Physics*, **2**, 1966: 314–320.

[6] SHANG, E.C. and ANDERSON, V.C. Surface-generated noise under low wind speed at kilohertz frequencies. *Journal of the Acoustical Society of America*, **79**, 1986: 964–971.

[7] CROWTHER, P.A. Near surface bubble excitation and noise in the ocean. *In*: INSTITUTE OF ACOUSTICS. UNDERWATER ACOUSTICS GROUP. Proceedings of the conference: Advances in Underwater Acoustics, Portland, Dorset, 1–2 December 1981. Edinburgh, Institute of Acoustics, 1981: pp. 12/1–12/7.

[8] BLAKE, W.K. Mechanics of Flow-Induced Sound and Vibration, volume I: General Concepts and Elementary Sources, volume II: Complex Flow-Structure Interactions. Orlando, FL, Academic Press, 1986: pp. 52–53 (I), 371–377 (I), 476–480 (II).

[9] STRASBERG, M. Gas bubbles as sources of sound in liquids. *Journal of the Acoustical Society of America*, **28**, 1956: 20–26.

[10] DEVIN, C. Survey of thermal, radiation, and viscous damping of pulsating air bubbles in water. *Journal of the Acoustical Society of America*, **31**, 1959: 1654–1667.

[11] LONGUET-HIGGINS, M.S. and TURNER, J.S. An 'entraining plume' model of a spilling breaker. *Journal of Fluid Mechanics*, **63**, 1974: 1–20.

[12] KUPERMAN, W.A. and INGENITO, F. Spatial correlation of surface generated noise in a stratified ocean. *Journal of the Acoustical Society of America*, **67**, 1980: 1988–1996.

[13] CRON, B.F. and SHERMAN, C.H. Spatial-correlation functions for various noise models. *Journal of the Acoustical Society of America*, **34**, 1962: 1732–1736.

[14] HAMSON, R.M. The theoretical responses of vertical and horizontal line arrays to wind-induced noise in shallow water. *Journal of the Acoustical Society of America*, **78**, 1985: 1702–1712.

[15] CROWTHER, P.A. Acoustical scattering from near-surface bubble layers. *In*: LAUTERBORN, W., *ed.* Cavitation and Inhomogeneities in Underwater Acoustics. Proceedings of the first international conference, Göttingen, 9–11 July, 1979. Berlin, Springer, 1980: pp. 194–204.

[16] MONAHAN, E.C. and ZIETLOW, C.R. Laboratory comparisons of fresh-water and salt-water whitecaps. *Journal of Geophysical Research*, **74**, 1969: 6961–6966.

[17] ROSS, D.B. and CARDONE, V. Observations of oceanic whitecaps and their relation to remote measurements of surface wind speed. *Journal of Geophysical Research*, **79**, 1974: 444–452.

Appendix A

The breaking-wave and bubble occurrences

In this appendix we obtain the multi-dimensional, non-homogeneous Poisson processes for the breaking-wave occurrences and the bubble occurrences. To this end we first summarize the relevant properties of a general Poisson process.

Points are said to be distributed in a space X according to a non-homogeneous Poisson process if for any subset A contained in X the number of points in A is a Poisson random variable N with the probability that n points lie in A given by

$$\Pr[N = n] = e^{-M} M^n / n!, \tag{A.1}$$

where

$$M = \int_A \lambda(\mathbf{x})\, \mathrm{d}^3\mathbf{x} \tag{A.2}$$

is the mean number of points in A and $\lambda(\mathbf{x})$ is the rate function (mean number of points per unit volume) of the process. Clearly, to specify a non-homogeneous Poisson process in the space X it suffices to specify its rate function $\lambda(\mathbf{x})$. In the special case where the rate function is independent of $\mathbf{x}$, the Poisson process is said to be homogeneous. In this case, M is given by

$$M = \lambda \mathrm{volume}(A). \tag{A.3}$$

Given that there are n points in A, the Poisson process describes those points in terms of a joint probability density given by

$$p(\mathbf{x}_1, \ldots, \mathbf{x}_n) = \prod_{k=1}^{n} p(\mathbf{x}_k), \tag{A.4a}$$

where

$$p(\mathbf{x}) = \begin{cases} \lambda(\mathbf{x})/M, & \mathbf{x} \in A \\ 0, & \text{otherwise.} \end{cases} \tag{A.4b}$$

It follows from Eqs. (A.4) that the points are independent, identically-distributed random variables with the common probability density of (A.4b).

The Poisson process for the breaking-wave occurrences is obtained by identifying the point $\mathbf{x}_k$ with $(\mathbf{r}_k, \tau_k)$ and taking A to be of the form $A = A_s \times \Theta$, where A_s is the total area of the ocean surface where breaking waves can occur and Θ is the time interval $[-\frac{1}{2}T, \frac{1}{2}T]$. It is assumed that during the time interval of interest the rate function depends only on the breaking-wave occurrence position $\mathbf{r}$ and not on the occurrence time. The number of breaking waves generated in the surface region A_s during the time interval Θ, N_w, has the probability function of (A.1) with mean

$$M_w = T \int_{A_s} \lambda(\mathbf{r})\, \mathrm{d}^2\mathbf{r}, \tag{A.5}$$

where the units of $\lambda(\mathbf{r})$ are whitecap occurrences per unit area per unit time. Furthermore, given that there are n breaking waves in A_s, the occurrence positions and times of those breaking waves are described in terms of the joint probability density

$$p(\mathbf{r}_1, \tau_1, \ldots, \mathbf{r}_n, \tau_n) = \prod_{k=1}^{n} p(\mathbf{r}_k, \tau_k), \tag{A.6a}$$

where

$$p(\mathbf{r}, \tau) = \begin{cases} \lambda(\mathbf{r})/M_w, & (\mathbf{r}, \tau) \in A_s \times \Theta \\ 0, & \text{otherwise.} \end{cases} \tag{A.6b}$$

The Poisson process for the bubble occurrences is obtained by identifying $\mathbf{x}_k$ with $(\mathbf{y}_k, \nu_k)$ and taking A to be of the form $A = V \times \Theta_{\mathbf{y}}$, where the bubble source region V is the total region swept out by the bubble generation region during the lifetime of the breaking wave and $\Theta_{\mathbf{y}}$ is the time interval during which the point $\mathbf{y} \in V$ is contained in the generation region. Thus, A represents the space-time set in which the bubbles are generated and hence the rate function $\mu(\mathbf{y}, \nu)$ is non-zero only for $(\mathbf{y}, \nu) \in A$. The number of bubbles generated in the source region during the lifetime of the breaking wave, N_b, has the probability function of (A.1) with mean

$$M_b = \int_V \int_{\Theta_{\mathbf{y}}} \mu(\mathbf{y}, \nu)\, d\nu\, d^3\mathbf{y}, \tag{A.7}$$

where $\mu(\mathbf{y}, \nu)$ has the units of bubble occurrences per unit volume per unit time. Given that there are n bubbles in A, the occurrence positions and times of those bubbles are described in terms of the joint probability density

$$p(\mathbf{y}_1, \nu_1, \ldots, \mathbf{y}_n, \nu_n) = \prod_{k=1}^{n} p(\mathbf{y}_k, \nu_k), \tag{A.8a}$$

where

$$p(\mathbf{y}, \nu) = \begin{cases} \mu(\mathbf{y}, \nu)/M_b, & (\mathbf{y}, \nu) \in V \times \Theta_{\mathbf{y}} \\ 0, & \text{otherwise.} \end{cases} \tag{A.8b}$$

Using (7a), the single-bubble occurrence density can also be written in the form

$$p(\mathbf{y}, \nu) = M_b^{-1} \mu(\mathbf{y}) \mu(\nu \mid \mathbf{y}), \tag{A.9a}$$

where

$$\mu(\nu \mid \mathbf{y}) = \mu(\mathbf{y}, \nu)/\mu(\mathbf{y}) \tag{A.9b}$$

is the conditional occurrence-time probability density. This probability density describes the bubble occurrence times at a fixed point within the total volume V.

Finally, from (A.9a) and the assumption that the bubble radius depends only on the occurrence position of the bubble and not on its occurrence time, the joint

probability density of the bubble occurrence position, its occurrence time and its radius can be written as

$$p(\mathbf{y}_1, \nu_1, R_1, \ldots, \mathbf{y}_n, \nu_n, R_n) = \prod_{k=1}^{n} p(\mathbf{y}_k, \nu_k, R_k), \tag{A.10a}$$

where

$$p(\mathbf{y}, \nu, R) = M_b^{-1} \mu(\mathbf{y}) \mu(\nu \mid \mathbf{y}) p(R \mid \mathbf{y}). \tag{A.10b}$$

Appendix B

Derivation of the noise cross-spectrum

Let $p(t;\mathbf{z})$ be the total pressure observed on a hydrophone located at position $\mathbf{z}$ due to the noise generated by the aggregate of breaking waves. We assume that the contributions from the individual breaking waves are statistically-independent, zero-mean processes with a common probability law that is independent of the position and the time at which the breaking wave occurs. Under this assumption, $p(t;\mathbf{z})$ can be written in the form

$$p(t;\mathbf{z}) = \sum_k p_w(t - \tau_k; \mathbf{r}_k, \mathbf{z}), \tag{B.1}$$

where $p_w(t - \tau_k; \mathbf{r}_k, \mathbf{z})$ is the pressure contribution from the kth breaking wave to occur, τ_k is the time at which the breaking wave begins, and $\mathbf{r}_k$ is its position on the ocean surface. The noise cross-spectrum between the pressures observed at positions $\mathbf{z}_1$ and $\mathbf{z}_2$ is defined as the fourier transform

$$C(\omega;\mathbf{z}_1,\mathbf{z}_2) = \int_{-\infty}^{\infty} R(t, t+u;\mathbf{z}_1,\mathbf{z}_2) e^{-i\omega u}\,\mathrm{d}u, \tag{B.2a}$$

where

$$R(t, t+u;\mathbf{z}_1,\mathbf{z}_2) = E[p(t;\mathbf{z}_1)p(t+u;\mathbf{z}_2)] \tag{B.2b}$$

is the space-time correlation function between the pressures at positions $\mathbf{z}_1$ and $\mathbf{z}_2$ and $E[\cdot]$ is the expected value operator over all stochastic variables determining the received pressure. Note that the noise cross-spectrum is well defined only when the space-time correlation function does not depend on the time t.

In this appendix we show that if the breaking-wave occurrence positions and occurence times $\{(\mathbf{r}_k, \tau_k)\}$ are described by the Poisson process specified in Eqs. (A.5) and (A.6) then the noise cross-spectrum is given by

$$C(\omega;\mathbf{z}_1,\mathbf{z}_2) = \int_{A_s} \lambda(\mathbf{r}) C_w(\omega;\mathbf{r},\mathbf{z}_1,\mathbf{z}_2)\,\mathrm{d}^2\mathbf{r}, \tag{B.3a}$$

where

$$C_w(\omega;\mathbf{r},\mathbf{z}_1,\mathbf{z}_2) = E_w[P_w^*(\omega;\mathbf{r},\mathbf{z}_1)P_w(\omega;\mathbf{r},\mathbf{z}_2)] \tag{B.3b}$$

is the breaking-wave cross-spectrum, $E_w[\cdot]$ is the expected value operator for fixed breaking-wave occurrence positions and occurrence times, and

$$P_w(\omega;\mathbf{r},\mathbf{z}_j) = \int_{-\infty}^{\infty} p_w(t;\mathbf{r},\mathbf{z}_j) e^{-i\omega t}\,\mathrm{d}t \tag{B.3c}$$

is the pressure spectrum resulting from an individual breaking wave. The noise intensity spectrum is obtained by setting $\mathbf{z}_1 = \mathbf{z}_2 = \mathbf{z}$ in Eqs. (B.3).

To establish Eqs. (B.3) it suffices to show that

$$R(t, t+u; \mathbf{z}_1, \mathbf{z}_2) = \int_{A_s} \lambda(\mathbf{r}) R_w(u; \mathbf{r}, \mathbf{z}_1, \mathbf{z}_2)\, d^2\mathbf{r}, \tag{B.4a}$$

where

$$R_w(u; \mathbf{r}, \mathbf{z}_1, \mathbf{z}_2) = \int_{-\infty}^{\infty} E_w[p_w(t; \mathbf{r}, \mathbf{z}_1) p_w(t+u; \mathbf{r}, \mathbf{z}_2)]\, dt. \tag{B.4b}$$

Given this result, (B.4a) can be used in (B.2a) to write the noise cross-spectrum in the form of (B.3a) where

$$C_w(\omega; \mathbf{r}, \mathbf{z}_1, \mathbf{z}_2) = \int_{-\infty}^{\infty} R_w(u; \mathbf{r}, \mathbf{z}_1, \mathbf{z}_2) e^{-i\omega u}\, du. \tag{B.5}$$

Eqs. (B.3b) and (B.3c) follow from using (B.4b) in (B.5).

To derive Eqs. (B.4), we first obtain an expression for the joint characteristic function of the random variables $p(t; \mathbf{z}_1)$ and $p(t+u; \mathbf{z}_2)$

$$\Phi(v_1, v_2) = E[e^{i(v_1 p(t;\mathbf{z}_1) + v_2 p(t+u;\mathbf{z}_2))}], \tag{B.6}$$

and then use the moment theorem

$$E[p(t; \mathbf{z}_1) p(t+u; \mathbf{z}_2)] = -\partial^2 \Phi(0,0)/\partial v_1 \partial v_2 \tag{B.7}$$

to determine the expected value in (B.2b). For notational convenience, we write $p(t; \mathbf{z}_1)$ and $p(t+u; \mathbf{z}_2)$ in the form

$$p(t; \mathbf{z}_1) = \sum_k p_{k,1}(\mathbf{r}_k, \tau_k), \tag{B.8a}$$

$$p(t+u; \mathbf{z}_2) = \sum_k p_{k,2}(\mathbf{r}_k, \tau_k), \tag{B.8b}$$

where

$$p_{k,1}(\mathbf{r}_k, \tau_k) = p_w(t - \tau_k; \mathbf{r}_k, \mathbf{z}_1), \tag{B.9a}$$

$$p_{k,2}(\mathbf{r}_k, \tau_k) = p_w(t + u - \tau_k; \mathbf{r}_k, \mathbf{z}_2). \tag{B.9b}$$

The characteristic function is obtained by expanding the expected value in (B.6) in terms of expected values conditioned on the event that there are exactly n breaking waves in the region $A = A_s \times \Theta$. The result is

$$\Phi(v_1, v_2) = \sum_{n=0}^{\infty} E[e^{i(v_1 p(t;\mathbf{z}_1) + v_2 p(t+u;\mathbf{z}_2))} \mid N_w = n] \Pr[N_w = n], \tag{B.10a}$$

where

$$E[e^{i(v_1 p(t;\mathbf{x}_1)+v_2 p(t+u;\mathbf{x}_2))} \mid N_w = n] = E_{\mathbf{r}_1,\tau_1,\ldots,\mathbf{r}_n,\tau_n}\left[E_w[e^{i(v_1 p(t;\mathbf{x}_1)+v_2 p(t+u;\mathbf{x}_2))}]\right], \tag{B.10b}$$

$\Pr[N_w = n]$ is given by (A.1) with M given by (A.5), and $E_{\mathbf{r}_1,\tau_1,\ldots,\mathbf{r}_n,\tau_n}[\cdot]$ is the expected value operator over the breaking-wave occurrence positions and occurrence times. Using Eqs. (B.8), the expected value in the nth term in the sum can be written as

$$\begin{aligned} E_{\mathbf{r}_1,\tau_1,\ldots,\mathbf{r}_n,\tau_n}&\left[E_w[e^{i(v_1 p(t;\mathbf{x}_1)+v_2 p(t+u;\mathbf{x}_2))}]\right] \\ &= E_{\mathbf{r}_1,\tau_1,\ldots,\mathbf{r}_n,\tau_n}\left[E_w[e^{i\sum_{k=1}^{n}(v_1 p_{k,1}+v_2 p_{k,2})}]\right] \\ &= E_{\mathbf{r}_1,\tau_1,\ldots,\mathbf{r}_n,\tau_n}\left[E_w[\prod_{k=1}^{n} e^{i(v_1 p_{k,1}+v_2 p_{k,2})}]\right] \\ &= \prod_{k=1}^{n} E_{\mathbf{r}_k,\tau_k}\left[E_w[e^{i(v_1 p_{k,1}+v_2 p_{k,2})}]\right] \\ &= \left(E_{\mathbf{r}_k,\tau_k}\left[E_w[e^{i(v_1 p_{k,1}+v_2 p_{k,2})}]\right]\right)^n, \end{aligned} \tag{B.11}$$

where we have used the fact that the points $\{(\mathbf{r}_k, \tau_k)\}$ are statistically independent and identically distributed to replace the expectation of the product by the product of the expectations in the third equation and to replace the product by the power in the last equation. Next, we write the outer expected value in the last equation as an integral using (A.6b) for the probability density. The result is

$$E_{\mathbf{r}_k,\tau_k}\left[E_w[e^{i(v_1 p_{k,1}+v_2 p_{k,2})}]\right] = \int_{-T/2}^{T/2}\int_{A_s} M_w^{-1}\lambda(\mathbf{r})E_w[e^{i(v_1 p_{k,1}+v_2 p_{k,2})}]\,d^2\mathbf{r}\,d\tau. \tag{B.12}$$

Using (B.12) in the last equation of (B.11) and then using the result in Eqs. (B.10) and substituting for $\Pr[N_w = n]$ using (A.1) yields

$$\Phi(v_1, v_2) = e^{-M_w}\sum_{n=0}^{\infty}\left(\int_{-T/2}^{T/2}\int_{A_s} M_w^{-1}\lambda(\mathbf{r})E_w[\,e^{i(v_1 p_{k,1}+v_2 p_{k,2})}]\,d^2\mathbf{r}\,d\tau\right)^n \times M_w^n/n!. \tag{B.13}$$

The desired expression for the characteristic function follows by writing the summation as an exponential function and using (A.5) to express M_w in terms of $\lambda(\mathbf{r})$. The result is

$$\Phi(v_1, v_2) = \exp\left(\int_{-T/2}^{T/2}\int_{A_s}\lambda(\mathbf{r})\left(E_w[e^{i(v_1 p_{k,1}+v_2 p_{k,2})}]-1\right)d^2\mathbf{r}\,d\tau\right). \tag{B.14}$$

Eqs. (B.4) are obtained by first using (B.14) to substitute for the characteristic function in (B.7), differentiating, setting $v_1 = v_2 = 0$ and using Eqs. (B.9) to substitute for $p_{k,1}$ and $p_{k,2}$. The result is

$$E[p(t;\mathbf{z}_1)p(t+u;\mathbf{z}_2)] = \int_{-T/2}^{T/2}\int_{A_s} \lambda(\mathbf{r})E_w[p_w(t-\tau;\mathbf{r},\mathbf{z}_1)p_w(t+u-\tau;\mathbf{r},\mathbf{z}_2)]\,\mathrm{d}^2\mathbf{r}\,\mathrm{d}\tau. \quad \text{(B.15)}$$

Interchanging the order of integration, making the change of variable $\tau' = t - \tau$, and taking the limit as T approaches infinity results in Eqs. (B.4).

Appendix C

Derivation of the breaking-wave cross-spectrum

In the previous appendix we derived the expression for the noise cross-spectrum in terms of the breaking-wave cross-spectrum. In this appendix we derive the expression for the breaking-wave cross-spectrum of (B.3b) under the assumptions of Sect. 2. For generality we allow the pressure transfer spectrum $H(\omega; \mathbf{y}, R)$ as well as the pressure excitation spectrum $F(\omega; \mathbf{y}, R)$ to be stochastic and define the single-bubble cross-spectrum $C_b(\omega; \mathbf{y}, \mathbf{y}', R, R')$ and the single-bubble spectrum $S_b(\omega; \mathbf{y}, R)$ by

$$C_b(\omega; \mathbf{y}, \mathbf{y}', R, R') = E_b[P_b^*(\omega; \mathbf{y}, R) P_b(\omega; \mathbf{y}', R')], \tag{C.1a}$$

and

$$S_b(\omega; \mathbf{y}, R) = E_b[|P_b(\omega; \mathbf{y}, R)|^2], \tag{C.1b}$$

where $E_b[\cdot]$ is the expected value operator for fixed bubble occurrence positions, occurrence times and radii. Note that when the pressure transfer spectrum is deterministic, $C_b(\omega; \mathbf{y}, \mathbf{y}', R, R')$ and $S_b(\omega; \mathbf{y}, R)$ are determined by the excitation cross-spectrum and the excitation energy spectrum of (6a) and (6b).

We show that under the assumptions of Sect. 2, the breaking-wave cross-spectrum is given by

$$\begin{aligned} C_w(\omega; \mathbf{r}, \mathbf{z}_1, \mathbf{z}_2) = &\int_V \mu(\mathbf{y}) S_{r.b.}(\omega; \mathbf{y}) G^*(\omega, \mathbf{r} + \mathbf{y}, \mathbf{z}_1) G(\omega, \mathbf{r} + \mathbf{y}, \mathbf{z}_2)\, \mathrm{d}^3\mathbf{y} \\ &+ \int_V \int_V \mu(\mathbf{y}) \mu(\mathbf{y}') C_{r.b.}(\omega; \mathbf{y}, \mathbf{y}') G^*(\omega, \mathbf{r} + \mathbf{y}, \mathbf{z}_1) G(\omega, \mathbf{r} + \mathbf{y}', \mathbf{z}_2) \\ &\times \Phi^*(\omega \mid \mathbf{y}) \Phi(\omega \mid \mathbf{y}')\, \mathrm{d}^3\mathbf{y}\, \mathrm{d}^3\mathbf{y}', \end{aligned} \tag{C.2a}$$

where

$$S_{r.b.}(\omega; \mathbf{y}) = \int_0^\infty S_b(\omega; \mathbf{y}, R) p(R \mid \mathbf{y})\, \mathrm{d}R \tag{C.2b}$$

is the radius-averaged bubble spectrum,

$$C_{r.b.}(\omega; \mathbf{y}, \mathbf{y}') = \int_0^\infty \int_0^\infty C_b(\omega; \mathbf{y}, \mathbf{y}', R, R') p(R \mid \mathbf{y}) p(R' \mid \mathbf{y}')\, \mathrm{d}R\, \mathrm{d}R' \tag{C.2c}$$

is the radius-averaged bubble cross-spectrum, and

$$\Phi(\omega \mid \mathbf{y}) = \int_{\Theta_\mathbf{y}} \mu(\nu \mid \mathbf{y}) e^{i\omega\nu}\, \mathrm{d}\nu \tag{C.2d}$$

is the characteristic function of the bubble occurrence-time probability density $\mu(\nu \mid \mathbf{y})$.

The cross-spectrum of (C.2a) is derived by expanding the expected value operator in (B.3b) as a sum of conditional expectations and then evaluating each term in the sum. The expansion has the form

$$C_{\mathrm{w}}(\omega;\mathbf{r},\mathbf{z}_1,\mathbf{z}_2) = \sum_{n=1}^{\infty} E_{\mathrm{w}}[P_{\mathrm{w}}^*(\omega;\mathbf{r},\mathbf{z}_1)P_{\mathrm{w}}(\omega;\mathbf{r},\mathbf{z}_2) \mid N_{\mathrm{b}} = n]\,\Pr[N_{\mathrm{b}} = n], \quad \text{(C.3a)}$$

where

$$E_{\mathrm{w}}[P_{\mathrm{w}}^*(\omega;\mathbf{r},\mathbf{z}_1)P_{\mathrm{w}}(\omega;\mathbf{r},\mathbf{z}_2) \mid N_{\mathrm{b}} = n] = E_{\mathbf{y}_1,\nu_1,R_1,\ldots,\mathbf{y}_n,\nu_n,R_n}\left[E_{\mathrm{b}}[P_{\mathrm{w}}^*(\omega;\mathbf{r},\mathbf{z}_1)P_{\mathrm{w}}(\omega;\mathbf{r},\mathbf{z}_2)]\right], \quad \text{(C.3b)}$$

$\Pr[N_{\mathrm{b}} = n]$ is given by (A.1) with M given by (A.7), and $E_{\mathbf{y}_1,\nu_1,R_1,\ldots,\mathbf{y}_n,\nu_n,R_n}[\cdot]$ is the expected value operator over the bubble occurrence positions, occurrence times and radii. To simplify the notation, we rewrite the expression for the spectrum of the received pressure (5) in the form

$$P_{\mathrm{w}}(\omega;\mathbf{r},\mathbf{z}_j) = \sum_{k=1}^{N_{\mathrm{b}}} P_{\mathrm{b}}(\mathbf{y}_k,R_k)G_j(\mathbf{y}_k)e^{i\omega\nu_k}, \quad \text{(C.4)}$$

where $P_{\mathrm{b}}(\mathbf{y},R)$ and $G_j(\mathbf{y})$ are the bubble pressure spectrum and the function $G(\omega, \mathbf{r}+\mathbf{y},\mathbf{z}_j)$ for fixed values of the frequency, the breaking-wave occurrence position and the hydrophone positions. Using (C.4) we write the inner expected value in (C.3b) in the form

$$E_{\mathrm{b}}[P_{\mathrm{w}}^*(\omega;\mathbf{r},\mathbf{z}_1)P_{\mathrm{w}}(\omega;\mathbf{r},\mathbf{z}_2)] = \sum_{k,k'=1}^{n} E_{\mathrm{b}}[(P_{\mathrm{b}}(\mathbf{y}_k,R_k)G_1(\mathbf{y}_k)e^{i\omega\nu_k})^* P_{\mathrm{b}}(\mathbf{y}_{k'},R_{k'})G_2(\mathbf{y}_{k'})e^{i\omega\nu_{k'}}]. \quad \text{(C.5)}$$

Rewriting the double summation in (C.5) as a sum over the diagonal terms and a sum over the off-diagonal terms and using the definitions of the single-bubble cross-spectrum and the single-bubble spectrum in Eqs. (C.1a) and (C.1b) results in

$$E_{\mathrm{b}}[P_{\mathrm{w}}^*(\omega;\mathbf{r},\mathbf{z}_1)P_{\mathrm{w}}(\omega;\mathbf{r},\mathbf{z}_2)] = \sum_{k=1}^{n} S_{\mathrm{b}}(\omega;\mathbf{y}_k,R_k)G_1^*(\mathbf{y}_k)G_2(\mathbf{y}_k) + \sum_{k\neq k'}^{n} C_{\mathrm{b}}(\omega;\mathbf{y}_k,\mathbf{y}_{k'},R_k,R_{k'})G_1^*(\mathbf{y}_k)G_2(\mathbf{y}_{k'}) \times e^{-i\omega\nu_k}e^{i\omega\nu_{k'}}. \quad \text{(C.6)}$$

Using (C.6) in (C.3b) and interchanging the expected value with the summation yields

$$
\begin{aligned}
&E_{\mathrm{w}}[P_{\mathrm{w}}^{*}(\omega;\mathbf{r},\mathbf{z}_1)P_{\mathrm{w}}(\omega;\mathbf{r},\mathbf{z}_2)\mid N_{\mathrm{b}}=n]\\
&\quad=\sum_{k=1}^{n}E_{\mathbf{y}_1,\nu_1,R_1,\ldots,\mathbf{y}_n,\nu_n,R_n}[S_{\mathrm{b}}(\omega;\mathbf{y}_k,R_k)G_1^{*}(\mathbf{y}_k)G_2(\mathbf{y}_k)]\\
&\qquad+\sum_{k\neq k'}^{n}E_{\mathbf{y}_1,\nu_1,R_1,\ldots,\mathbf{y}_n,\nu_n,R_n}[C_{\mathrm{b}}(\omega;\mathbf{y}_k,\mathbf{y}_{k'},R_k,R_{k'})G_1^{*}(\mathbf{y}_k)G_2(\mathbf{y}_{k'})e^{-i\omega\nu_k}e^{i\omega\nu_{k'}}]\\
&\quad=\sum_{k=1}^{n}E_{\mathbf{y}_k,\nu_k,R_k}[S_{\mathrm{b}}(\omega;\mathbf{y}_k,R_k)G_1^{*}(\mathbf{y}_k)G_2(\mathbf{y}_k)]\\
&\qquad+\sum_{k\neq k'}^{n}E_{\mathbf{y}_k,\nu_k,R_k,\mathbf{y}_{k'},\nu_{k'},R_{k'}}[C_{\mathrm{b}}(\omega;\mathbf{y}_k,\mathbf{y}_{k'},R_k,R_{k'})G_1^{*}(\mathbf{y}_k)G_2(\mathbf{y}_{k'})\\
&\qquad\qquad\times e^{-i\omega\nu_k}e^{i\omega\nu_{k'}}].
\end{aligned}
\tag{C.7}
$$

Using the joint probability density for $(\mathbf{y}_k,\nu_k,R_k)$ of (A.10b), the first expected value in (C.7) can be written as

$$
\begin{aligned}
&E_{\mathbf{y}_k,\nu_k,R_k}[S_{\mathrm{b}}(\omega;\mathbf{y}_k,R_k)G_1^{*}(\mathbf{y}_k)G_2(\mathbf{y}_k)]\\
&\quad=\int M_{\mathrm{b}}^{-1}\mu(\mathbf{y}_k)\mu(\nu_k\mid\mathbf{y}_k)p(R_k\mid\mathbf{y}_k)S_{\mathrm{b}}(\omega;\mathbf{y}_k,R_k)G_1^{*}(\mathbf{y}_k)G_2(\mathbf{y}_k)\,\mathrm{d}^3\mathbf{y}_k\,\mathrm{d}\nu_k\,\mathrm{d}R_k\\
&\quad=M_{\mathrm{b}}^{-1}\int_V\mu(\mathbf{y})S_{\mathrm{r.b.}}(\omega;\mathbf{y})G_1^{*}(\mathbf{y})G_2(\mathbf{y})\,\mathrm{d}^3\mathbf{y},
\end{aligned}
\tag{C.8a}
$$

where $S_{\mathrm{r.b.}}(\omega;\mathbf{y})$ is the radius-averaged bubble spectrum of (C.2b). Similarly, the second expected value in (C.7) can be written as

$$
\begin{aligned}
&E_{\mathbf{y}_k,\nu_k,R_k,\mathbf{y}_{k'},\nu_{k'},R_{k'}}[C_{\mathrm{b}}(\omega;\mathbf{y}_k,\mathbf{y}_{k'},R_k,R_{k'})G_1^{*}(\mathbf{y}_k)G_2(\mathbf{y}_{k'})e^{-i\omega\nu_k}e^{i\omega\nu_{k'}}]\\
&\qquad=\int\int M_{\mathrm{b}}^{-2}\mu(\mathbf{y}_k)\mu(\nu_k\mid\mathbf{y}_k)p(R_k\mid\mathbf{y}_k)\mu(\mathbf{y}_{k'})\mu(\nu_{k'}\mid\mathbf{y}_{k'})p(R_{k'}\mid\mathbf{y}_{k'})\\
&\qquad\qquad\times C_{\mathrm{b}}(\omega;\mathbf{y}_k,\mathbf{y}_{k'},R_k,R_{k'})G_1^{*}(\mathbf{y}_k)G_2(\mathbf{y}_{k'})\\
&\qquad\qquad\times e^{-i\omega\nu_k}e^{i\omega\nu_{k'}}\,\mathrm{d}^3\mathbf{y}_k\,\mathrm{d}\nu_k\,\mathrm{d}R_k\,\mathrm{d}^3\mathbf{y}_{k'}\,\mathrm{d}\nu_{k'}\,\mathrm{d}R_{k'}\\
&\qquad=M_{\mathrm{b}}^{-2}\int_V\int_V\mu(\mathbf{y})\mu(\mathbf{y}')C_{\mathrm{r.b.}}(\omega;\mathbf{y},\mathbf{y}')G_1^{*}(\mathbf{y})G_2(\mathbf{y}')\\
&\qquad\qquad\times\Phi^{*}(\omega\mid\mathbf{y})\Phi(\omega\mid\mathbf{y}')\,\mathrm{d}^3\mathbf{y}\,\mathrm{d}^3\mathbf{y}',
\end{aligned}
\tag{C.8b}
$$

where $C_{\mathrm{r.b.}}(\omega;\mathbf{y},\mathbf{y}')$ is the radius-averaged bubble cross-spectrum of (C.2c) and $\Phi(\omega\mid\mathbf{y})$ is the characteristic function of (C.2d). Using (C.8a) and (C.8b) in (C.7)

and evaluating the summation yields

$$E_w[P_w^*(\omega;\mathbf{r},\mathbf{z}_1)P_w(\omega;\mathbf{r},\mathbf{z}_2) \mid N_b = n] =$$
$$nM_b^{-1}\int_V \mu(\mathbf{y})S_{r.b.}(\omega;\mathbf{y})G_1^*(\mathbf{y})G_2(\mathbf{y})\,d^3\mathbf{y}$$
$$+ n(n-1)M_b^{-2}\int_V\int_V \mu(\mathbf{y})\mu(\mathbf{y}')C_{r.b.}(\omega;\mathbf{y},\mathbf{y}')G_1^*(\mathbf{y})G_2(\mathbf{y}')$$
$$\times \Phi^*(\omega \mid \mathbf{y})\Phi(\omega \mid \mathbf{y}')\,d^3\mathbf{y}\,d^3\mathbf{y}'. \qquad (C.9)$$

Finally, using (C.9) in (C.3a) and the facts that

$$M_b = \sum_{n=1}^{\infty} n\,\Pr[N_b = n] \qquad (C.10a)$$

and for a Poisson random variable

$$M_b(M_b+1) = \sum_{n=1}^{\infty} n^2\,\Pr[N_b = n] \qquad (C.10b)$$

yields (C.2a).

Appendix D

The high-frequency approximation

The breaking-wave energy spectrum is obtained from (C.2a) by setting $\mathbf{z}_1 = \mathbf{z}_2 = \mathbf{z}$. The result can be written in the form

$$S_{\mathrm{w}}(\omega; \mathbf{r}, \mathbf{z}) = S_{\mathrm{w1}}(\omega; \mathbf{r}, \mathbf{z}) + S_{\mathrm{w2}}(\omega; \mathbf{r}, \mathbf{z}), \tag{D.1a}$$

where

$$S_{\mathrm{w1}}(\omega; \mathbf{r}, \mathbf{z}) = \int_V \mu(\mathbf{y}) S_{\mathrm{r.b.}}(\omega; \mathbf{y}) |G(\omega, \mathbf{r} + \mathbf{y}, \mathbf{z})|^2 \, \mathrm{d}^3\mathbf{y}, \tag{D.1b}$$

$$S_{\mathrm{w2}}(\omega; \mathbf{r}, \mathbf{z}) = \int_V \int_V \mu(\mathbf{y}) \mu(\mathbf{y}') C_{\mathrm{r.b.}}(\omega; \mathbf{y}, \mathbf{y}') G^*(\omega, \mathbf{r} + \mathbf{y}, \mathbf{z}) G(\omega, \mathbf{r} + \mathbf{y}', \mathbf{z})$$

$$\times \Phi^*(\omega \mid \mathbf{y}) \Phi(\omega \mid \mathbf{y}') \, \mathrm{d}^3\mathbf{y} \, \mathrm{d}^3\mathbf{y}'. \tag{D.1c}$$

In this appendix we derive a frequency-dependent upper bound on the ratio of the second term in (D.1a) to the first and use that bound to identify the frequencies where the contributions of the second term can be neglected.

The upper bound depends only on the mean number of bubbles generated in the breaking wave and the probability density of the bubble occurrence times. As such it is completely determined by the bubble generation rate function $\mu(\mathbf{y}, \nu)$. The formal statement of the upper bound is as follows. Let $\rho(\omega)$ be defined by

$$\rho(\omega) = M_{\mathrm{b}} |\Phi(\omega \mid \mathbf{y}_0)|^2, \tag{D.2a}$$

where $\Phi(\omega \mid \mathbf{y})$ is the characteristic function of the probability density $\mu(\nu \mid \mathbf{y})$ and $\mathbf{y}_0(\omega)$ is determined by

$$|\Phi(\omega \mid \mathbf{y}_0(\omega))|^2 = \max_{\mathbf{y} \in \mathbf{V}} |\Phi(\omega \mid \mathbf{y})|^2. \tag{D.2b}$$

Then the spectra $S_{\mathrm{w1}}(\omega; \mathbf{r}, \mathbf{z})$ and $S_{\mathrm{w2}}(\omega; \mathbf{r}, \mathbf{z})$ satisfy

$$|S_{\mathrm{w2}}(\omega; \mathbf{r}, \mathbf{z})| \leq \rho(\omega) S_{\mathrm{w1}}(\omega; \mathbf{r}, \mathbf{z}). \tag{D.2c}$$

To apply the upper bound, we consider the special case where the bubble generation region has fixed dimensions and moves with constant speed. We further assume that the bubbles in this region are generated at a constant rate. For this case, $\mu(\mathbf{y}, \nu)$ is constant for each $\nu \in \Theta_{\mathbf{y}}$ and $\Theta_{\mathbf{y}}$ is independent of $\mathbf{y} \in V$. It follows from (A.9b) that $\mu(\nu \mid \mathbf{y})$ is a uniform probability density for each $\nu \in \Theta_{\mathbf{y}}$. Thus by using the

expression for the characteristic function of a uniform random variable in (D.2a) we obtain

$$\rho(\omega) = M_b \left(\frac{\sin(\frac{1}{2}\omega T)}{\frac{1}{2}\omega T} \right)^2 \leq \frac{M_b}{(\frac{1}{2}\omega T)^2}, \tag{D.3}$$

where T is the duration of the interval Θ_y. For $M_b = 10^4$ bubbles and $T = 0.1$ s, $\rho \leq 0.1$ for frequencies $f \geq 1$ kHz. Thus, for the high frequencies of interest, the energy spectrum is well approximated by the first term of (D.1a).

The derivation of the upper bound makes use of the following property of expected value operators. Let X and Y be two complex random variables. Then

$$|E[XY]| \leq E[|XY|] \leq (E[|X|^2])^{1/2} (E[|Y|^2])^{1/2} \tag{D.4a}$$

and

$$E[|X|^{1/2}] \leq (E[|X|])^{1/2}. \tag{D.4b}$$

The inequality (D.4a) is simply an application of Cauchy's inequality where the inner product is the expectation operator. The inequality (D.4b) is obtained from (D.4a) by setting $Y = 1$ and using $|X|^{1/2}$ in place of $|X|$.

To derive the upper bound, we first show that the magnitude of the radius-averaged cross-spectrum satisfies

$$|C_{r.b.}(\omega; \mathbf{y}, \mathbf{y}')| \leq (S_{r.b.}(\omega; \mathbf{y}) S_{r.b.}(\omega; \mathbf{y}'))^{1/2}. \tag{D.5}$$

To this end we rewrite (C.2c) in the form

$$C_{r.b.}(\omega; \mathbf{y}, \mathbf{y}') = \int_0^\infty \int_0^\infty (S_b(\omega; \mathbf{y}, R) S_b(\omega; \mathbf{y}', R'))^{1/2} \hat{C}_b(\omega; \mathbf{y}, \mathbf{y}', R, R') \times p(R \mid \mathbf{y}) p(R' \mid \mathbf{y}') \, dR \, dR', \tag{D.6a}$$

where

$$\hat{C}_b(\omega; \mathbf{y}, \mathbf{y}', R, R') = \frac{C_b(\omega; \mathbf{y}, \mathbf{y}', R, R')}{(S_b(\omega; \mathbf{y}, R) S_b(\omega; \mathbf{y}', R'))^{1/2}} \tag{D.6b}$$

is the normalized single-bubble cross-spectrum. By applying (D.4a) to $C_b(\omega; \mathbf{y}, \mathbf{y}', R, R') = E_b[P_b^*(\omega; \mathbf{y}, R) P_b(\omega; \mathbf{y}', R')]$, and then using the result in (D.6b), we obtain

$$|\hat{C}_b(\omega; \mathbf{y}, \mathbf{y}', R, R')| \leq 1. \tag{D.7}$$

Taking the magnitude of both sides of (D.6a) and using (D.7) results in

$$|C_{\text{r.b.}}(\omega;\mathbf{y},\mathbf{y}')| \le \int_0^\infty (S_{\text{b}}(\omega;\mathbf{y},R))^{1/2}\, p(R \mid \mathbf{y})\,\mathrm{d}R \times \int_0^\infty (S_{\text{b}}(\omega;\mathbf{y}',R))^{1/2}\, p(R \mid \mathbf{y}')\,\mathrm{d}R. \tag{D.8}$$

Applying (D.4b) to both integrals on the rhs of (D.8) with $|X|$ equal to $S_{\text{b}}(\omega;\mathbf{y},R)$ and $S_{\text{b}}(\omega;\mathbf{y}',R)$ respectively we obtain

$$|C_{\text{r.b.}}(\omega;\mathbf{y},\mathbf{y}')| \le \left(\int_0^\infty S_{\text{b}}(\omega;\mathbf{y},R)p(R \mid \mathbf{y})\,\mathrm{d}R\right)^{1/2} \times \left(\int_0^\infty S_{\text{b}}(\omega;\mathbf{y}',R)p(R \mid \mathbf{y}')\,\mathrm{d}R\right)^{1/2}. \tag{D.9}$$

The inequality (D.5) follows immediately from (D.9) and the definition of the radius-averaged bubble spectrum (C.2b).

We now complete the derivation. By taking the magnitude of both sides of (D.1c) and using (D.5) we obtain

$$S_{\text{w2}}(\omega;\mathbf{r},\mathbf{z}) \le \int_V \int_V \mu(\mathbf{y})\mu(\mathbf{y}')\,(S_{\text{r.b.}}(\omega;\mathbf{y})S_{\text{r.b.}}(\omega;\mathbf{y}'))^{1/2}\,|G^*(\omega,\mathbf{r}+\mathbf{y},\mathbf{z}) \times G(\omega,\mathbf{r}+\mathbf{y}',\mathbf{z})\Phi^*(\omega \mid \mathbf{y})\Phi(\omega \mid \mathbf{y}')|\,\mathrm{d}^3\mathbf{y}\,\mathrm{d}^3\mathbf{y}'. \tag{D.10}$$

The double integral on the rhs of (D.10) separates into a product of two integrals. Using this we rewrite (D.10) in the form

$$S_{\text{w2}}(\omega;\mathbf{r},\mathbf{z}) \le \left(\int_V \mu(\mathbf{y})\,(S_{\text{r.b.}}(\omega;\mathbf{y}))^{1/2}\,|G(\omega,\mathbf{r}+\mathbf{y},\mathbf{z})||\Phi(\omega \mid \mathbf{y})|\,\mathrm{d}^3\mathbf{y}\right)^2. \tag{D.11}$$

By rearranging the integrand in (D.11) and using the fact that $M_{\text{b}}^{-1}\mu(\mathbf{y})$ is a probability density we can write

$$S_{\text{w2}}(\omega;\mathbf{r},\mathbf{z}) \le M_{\text{b}}^2 \left(E[(|S_{\text{r.b.}}(\omega;\mathbf{y})||G(\omega,\mathbf{r}+\mathbf{y},\mathbf{z})|^2|\Phi(\omega \mid \mathbf{y})|^2)^{1/2}]\right)^2, \tag{D.12}$$

where $E[\cdot]$ is the expectation with respect to the probability density $M_{\text{b}}^{-1}\mu(\mathbf{y})$. Applying the inequality (D.4b) to (D.12) results in

$$S_{\text{w2}}(\omega;\mathbf{r},\mathbf{z}) \le M_{\text{b}}^2 E[|S_{\text{r.b.}}(\omega;\mathbf{y})||G(\omega,\mathbf{r}+\mathbf{y},\mathbf{z})|^2|\Phi(\omega \mid \mathbf{y})|^2]. \tag{D.13}$$

Using (D.2b) to bound the rhs of (D.13) we obtain

$$S_{\text{w2}}(\omega;\mathbf{r},\mathbf{z}) \le M_{\text{b}}^2 E[|S_{\text{r.b.}}(\omega;\mathbf{y})||G(\omega,\mathbf{r}+\mathbf{y},\mathbf{z})|^2]|\Phi(\omega \mid \mathbf{y}_0(\omega))|^2. \tag{D.14}$$

Finally, by expressing the integral on the rhs of (D.1b) in terms of the expected value operator $E[\cdot]$, we obtain

$$S_{\text{w1}}(\omega;\mathbf{r},\mathbf{z}) = M_{\text{b}} E[|S_{\text{r.b.}}(\omega;\mathbf{y})||G(\omega,\mathbf{r}+\mathbf{y},\mathbf{z})|^2]. \tag{D.15}$$

The upper bound follows immediately by using (D.15) in (D.14).

Appendix E

The model equations for the examples of Sect. 5

The breaking-wave energy spectrum and the noise intensity spectrum describe the noise observed on a single hydrophone located at the position $\mathbf{z}$. In the simplified model for the ideal medium (homogeneous, semi-infinite), the breaking-wave energy spectrum is given by

$$S_{\mathrm{w}}(\omega;\mathbf{r},\mathbf{z}) = M_{\mathrm{b}} S_{\mathrm{m.b.}}(\omega) R(\omega,\theta) T(\omega,|\mathbf{z}-\mathbf{r}|), \tag{E.1a}$$

and the noise intensity spectrum is given by

$$S(\omega;\mathbf{z}) = \lambda M_{\mathrm{b}} S_{\mathrm{m.b.}}(\omega) C_{\mathrm{i}}'(\omega;z,0,\gamma). \tag{E.1b}$$

The transmission loss $T(\omega,|\mathbf{z}-\mathbf{r}|)$ is determined by (14c) and the integrated spectrum $C_{\mathrm{i}}'(\omega;z,0,\gamma)$ is determined by (15b) with the hydrophone separation z' set equal to zero. The mean bubble spectrum $S_{\mathrm{m.b.}}(\omega)$ and the radiation pattern $R(\omega,\theta)$ depend on the mechanism by which the bubble vibrations are excited. In this appendix we derive the equations that determine the mean bubble spectrum and the radiation pattern for the excitation postulates of Sect. 4 and the assumption that the pressure transfer spectrum $H(\omega;\mathbf{y},R)$, the bubble generation rate $\mu(\mathbf{y})$ and the bubble-radius density $p(R \mid \mathbf{y})$ are independent of $\mathbf{y}$ throughout the source region.

For the pressure-jump excitation the radius-averaged bubble spectrum $S_{\mathrm{r.b.}}(\omega;\mathbf{y})$ is obtained from (8c) with the single-bubble spectrum $S_{\mathrm{b}}(\omega;\mathbf{y},R)$ obtained from (8d) using the excitation energy spectrum of (18b). Making these substitutions and noting that $S_F(\omega;\mathbf{y},R)$ is independent of R results in

$$S_{\mathrm{r.b.}}(\omega;\mathbf{y}) = E[|H(\omega;R)|^2]\,(\rho g d(\mathbf{y})/\omega)^2, \tag{E.2}$$

where $E[\cdot]$ is the expectation with respect to $p(R)$. The mean bubble spectrum is obtained by using (E.2) in (8b). The result is

$$\begin{aligned} S_{\mathrm{m.b.}}(\omega) &= \int_V E[|H(\omega;R)|^2]\,(\rho g d(\mathbf{y})/\omega)^2 M_{\mathrm{b}}^{-1}\mu(\mathbf{y})\,\mathrm{d}^3\mathbf{y} \\ &= E[|H(\omega;R)|^2](\rho g/\omega)^2 \int_V (d(\mathbf{y}))^2 M_{\mathrm{b}}^{-1}\mu(\mathbf{y})\,\mathrm{d}^3\mathbf{y} \end{aligned}$$

or equivalently

$$S_{\mathrm{m.b.}}(\omega) = S_{\mathrm{r.b.}}(\omega;D'), \tag{E.3a}$$

where $S_{\mathrm{r.b.}}(\omega;D')$ is the radius-averaged bubble spectrum evaluated at $d(\mathbf{y}) = D'$, and

$$D' = \left(\int_V (d(\mathbf{y}))^2 M_{\mathrm{b}}^{-1}\mu(\mathbf{y})\,\mathrm{d}^3\mathbf{y}\right)^{1/2} \tag{E.3b}$$

is the rms source depth.

The normalized radius-averaged spectrum $\hat{S}_{\text{r.b.}}(\omega;\mathbf{y})$ is obtained by using (E.2) in (8f). The result is

$$\hat{S}_{\text{r.b.}}(\omega;\mathbf{y}) = M_{\text{b}}^{-1}\mu(\mathbf{y})E[|H(\omega;R)|^2](\rho g d(\mathbf{y})/\omega)^2/S_{\text{m.b.}}(\omega)$$

or, alternatively, using Eqs. (E.3)

$$\hat{S}_{\text{r.b.}}(\omega;\mathbf{y}) = M_{\text{b}}^{-1}\mu(\mathbf{y})(d(\mathbf{y}))^2/(D')^2. \tag{E.4}$$

In the simplified model the source region has a horizontal cross-section A' that is independent of depth so that

$$d(\mathbf{y}) = y'', \tag{E.5a}$$

and for the special case where $\mu(\mathbf{y})$ is constant

$$\mu(\mathbf{y}) = M_{\text{b}}/(A'D). \tag{E.5b}$$

It follows from (E.3b) and Eqs. (E.5) that D' is given by

$$D' = \left(D^{-1}\int_0^D (y'')^2\,dy''\right)^{1/2} = 0.58D, \tag{E.6}$$

and from (12c), (E.4) and Eqs. (E.5) that $\hat{S}_{\text{r.b.}}(\omega;y'')$ is

$$\hat{S}_{\text{r.b.}}(\omega;y'') = D^{-1}(y'')^2/(D')^2. \tag{E.7}$$

The radiation pattern is obtained by using (E.7) in (14b). The result is

$$R(\omega,\theta) = D^{-1}(D')^{-2}\int_0^D (y'')^2\,(2\sin((\omega/c)\cos(\theta)y''))^2\,dy''. \tag{E.8}$$

For the volume-rate excitation the radius-averaged bubble spectrum is obtained from (8c), (8d) and (19b). The result is

$$S_{\text{r.b.}}(\omega;\mathbf{y}) = E[|H(\omega;R)|^2R^2](\rho U')^2. \tag{E.9}$$

Since the rhs of (E.9) is independent of $\mathbf{y}$, the mean bubble spectrum is also given by (E.9) and the normalized radius-averaged spectrum is simply

$$\hat{S}_{\text{r.b.}}(\omega;\mathbf{y}) = M_{\text{b}}^{-1}\mu(\mathbf{y}). \tag{E.10}$$

For the simplified model with $\mu(\mathbf{y})$ constant throughout the source region, it follows from (12c), (E.10) and Eqs. (E.5) that $\hat{S}_{\text{r.b.}}(\omega;y'')$ is

$$\hat{S}_{\text{r.b.}}(\omega;y'') = D^{-1}, \tag{E.11}$$

and from (14b) and (E.11) that the radiation pattern is

$$R(\omega,\theta) = D^{-1}\int_0^D (2\sin((\omega/c)\cos(\theta)y''))^2\,dy''. \tag{E.12}$$

Initial Distribution for SR-145

Ministries of Defence	
JSPHQ Belgium	2
DND Canada	10
CHOD Denmark	8
MOD France	8
MOD Germany	15
MOD Greece	11
MOD Italy	10
MOD Netherlands	12
CHOD Norway	10
MOD Portugal	2
MOD Spain	2
MOD Turkey	5
MOD UK	20
SECDEF US	68
NATO Authorities	
Defence Planning Committee	3
NAMILCOM	2
SACLANT	3
SACLANTREPEUR	1
CINCWESTLANT/ COMOCEANLANT	1
COMSTRIKFLTANT	1
CINCIBERLANT	1
CINCEASTLANT	1
COMSUBACLANT	1
COMMAIREASTLANT	1
SACEUR	2
CINCNORTH	1
CINCSOUTH	1
COMNAVSOUTH	1
COMSTRIKFORSOUTH	1
COMEDCENT	1
COMMARAIRMED	1
CINCHAN	3
SCNR for SACLANTCEN	
SCNR Belgium	1
SCNR Canada	1
SCNR Denmark	1
SCNR Germany	1
SCNR Greece	1
SCNR Italy	1
SCNR Netherlands	1
SCNR Norway	1
SCNR Portugal	1
SCNR Turkey	1
SCNR UK	1
SCNR US	2
French Delegate	1
SECGEN Rep. SCNR	1
NAMILCOM Rep. SCNR	1
National Liaison Officers	
NLO Canada	1
NLO Denmark	1
NLO Germany	1
NLO Italy	1
NLO UK	1
NLO US	1
NLR to SACLANT	
NLR Belgium	1
NLR Canada	1
NLR Denmark	1
NLR Germany	1
NLR Greece	1
NLR Italy	1
NLR Netherlands	1
NLR Norway	1
NLR Portugal	1
NLR Turkey	1
NLR UK	1
Total external distribution	250
SACLANTCEN Library	10
Stock	20
Total number of copies	280